

General formulation of spin-flip time-dependent density functional theory using non-collinear kernels: Theory, implementation, and benchmarks

Yves A. Bernard, Yihan Shao, and Anna I. Krylov

Citation: *J. Chem. Phys.* **136**, 204103 (2012); doi: 10.1063/1.4714499

View online: <http://dx.doi.org/10.1063/1.4714499>

View Table of Contents: <http://jcp.aip.org/resource/1/JCPSA6/v136/i20>

Published by the [American Institute of Physics](#).

Additional information on *J. Chem. Phys.*

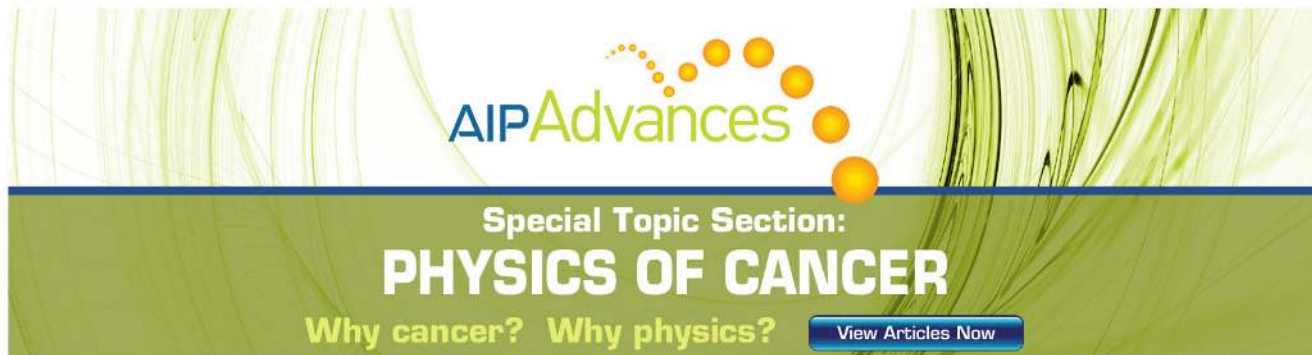
Journal Homepage: <http://jcp.aip.org/>

Journal Information: http://jcp.aip.org/about/about_the_journal

Top downloads: http://jcp.aip.org/features/most_downloaded

Information for Authors: <http://jcp.aip.org/authors>

ADVERTISEMENT



AIP Advances

Special Topic Section:
PHYSICS OF CANCER

Why cancer? Why physics? [View Articles Now](#)

General formulation of spin-flip time-dependent density functional theory using non-collinear kernels: Theory, implementation, and benchmarks

Yves A. Bernard,¹ Yihan Shao,² and Anna I. Krylov^{1,a)}¹Department of Chemistry, University of Southern California, Los Angeles, California 90089-0482, USA²Q-Chem Inc., 5001 Baum Blvd, Suite 690, Pittsburgh, Pennsylvania 15213, USA

(Received 19 March 2012; accepted 25 April 2012; published online 23 May 2012)

We report an implementation of the spin-flip (SF) variant of time-dependent density functional theory (TD-DFT) within the Tamm-Dancoff approximation and non-collinear (NC) formalism for local, generalized gradient approximation, hybrid, and range-separated functionals. The performance of different functionals is evaluated by extensive benchmark calculations of energy gaps in a variety of diradicals and open-shell atoms. The benchmark set consists of 41 energy gaps. A consistently good performance is observed for the Perdew-Burke-Ernzerhof (PBE) family, in particular PBE0 and PBE50, which yield mean average deviations of 0.126 and 0.090 eV, respectively. In most cases, the performance of original (collinear) SF-TDDFT with 50-50 functional is also satisfactory (as compared to non-collinear variants), except for the same-center diradicals where both collinear and non-collinear SF variants that use LYP or B97 exhibit large errors. The accuracy of NC-SF-TDDFT and collinear SF-TDDFT with 50-50 and BHHLYP is very similar. Using PBE50 within collinear formalism does not improve the accuracy. © 2012 American Institute of Physics. [<http://dx.doi.org/10.1063/1.4714499>]

I. INTRODUCTION

Electronic degeneracy, which is ubiquitous in chemistry, presents a challenge to *ab initio* methodology as it leads to multi-configurational wave functions. Well-known examples include electronically excited and open-shell species (radicals, diradicals, triradicals, etc.), as well as molecules with stretched bonds, i.e., at the dissociation limit or transition states. In these cases, the well-developed hierarchy of ground-state methods^{1,2} based on the assumption that the wave function is dominated by a single Slater determinant breaks down, as the Hartree-Fock method fails to provide a qualitatively correct zero-order description. Kohn-Sham (KS) density functional theory (DFT) with inexact functionals also fails, although in principle a single Kohn-Sham determinant can represent the exact density corresponding to a multi-configurational wave function.

Yet, many of these “multi-reference” situations can be efficiently described by robust and efficient single-reference approaches based on equation-of-motion (EOM) or linear response (LR) formalisms.³ For example, excited states (Ψ_{ex}) are described as linear combination of determinants that are “excited” with respect to the ground-state wave function (Ψ_0),

$$\Psi_{ex} = \hat{R}\Psi_0, \quad (1)$$

where the exact form of an excitation operator \hat{R} depends on a ground-state wave function employed. For example, when Ψ_0 is just a Hartree-Fock (HF) determinant (Φ_0), the operator \hat{R} generates all singly excited determinants (Φ_i^a) leading to the configuration interaction singles (CIS) method (see

Fig. 1). The coefficients r_i^a are found by diagonalizing the Hamiltonian on the basis of $\{\Phi_i^a\}$.

Using higher-level reference wave functions (e.g., coupled-cluster with single and double substitutions, CCSD) lead to operator \hat{R} that generates all singly and doubly excited (with respect to Φ_0) determinants giving rise to equation-of-motion or linear response CCSD (EOM-CCSD or LR-CCSD) method.³⁻⁹

Linear response within KS-DFT leads to equations that are identical to those of CIS, or random phase approximation (RPA) if Tamm-Dancoff approximation (TDA) is not invoked. Although the meaning of excited determinants is somewhat different in TD-DFT as compared to CIS, i.e., they are only representing the change in the electronic density upon electronic excitation and not the excited-state wave function itself, it is still operationally useful to analyze TD-DFT expansions in a fashion similar to that of the wave function based methods.

As clearly illustrated in Fig. 1, this form of a wave function is capable of describing, for example, two-configurational open-shell excited states for which two determinants are required for spin-adaptation, e.g., for an excited state of a $\pi\pi^*$ character, $\Psi_{ex} \sim |\pi\alpha\pi^*\beta\rangle \pm |\pi\beta\pi^*\alpha\rangle$. Furthermore, states of a mixed character such as $\pi\pi^*$ mixed with $n\pi^*$ or Rydberg-type $\pi 3s(Ry)$ configurations can also be correctly represented by a CIS-like ansatz, Eq. (1). However, the limitation of this representation becomes obvious when one considers states of a doubly excited character [e.g., $(\pi^*)^2$ in ethylene or dark states in polyenes]—such doubly excited determinants are simply absent in the CIS or TD-DFT expansions. Doubly excited states often become important in the situations when the ground-state wave function acquires multi-configurational character, e.g., as in diradicals, at transition

^{a)} Author to whom correspondence should be addressed. Electronic mail: krylov@usc.edu.

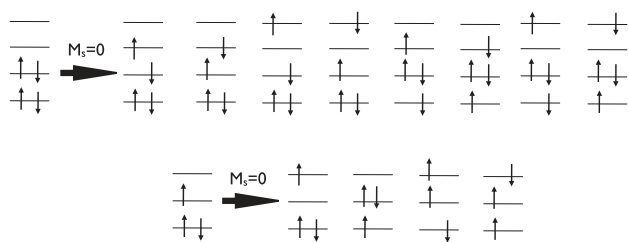


FIG. 1. Target determinants generated by spin-conserving ($M_s = 0$) excitation operator from a singlet (top) or a doublet (bottom) reference in the CIS or TD-DFT/TDA methods.

states, or at conical intersections. Similar problems arise in excited states of doublet radicals— as one can see from Fig. 1 (bottom), the set of determinants generated by strictly single excitations from a doublet reference is not spin-complete and the missing bit is formally a double excitation.¹⁰

The spin-flip (SF) approach offers a simple and efficient solution to this sort of electronic structure.^{11–16} SF methods employ a high-spin reference state, which is accurately described by a single-reference wave function. For example, in diradicals (or at transition states) where the singlet state HOMO and LUMO (highest occupied and lowest unoccupied molecular orbitals) are (nearly) degenerate, the respective high-spin ($\alpha\alpha$) triplet state is perfectly well behaved as both nearly degenerate orbitals are occupied. Likewise, high-spin quartet triradical states ($\alpha\alpha\alpha$) can also be well described by a single-determinantal ansatz. The problematic target states, such as closed- and open-shell singlets (and triplets) in diradicals or bond-breaking, are then described as spin-flipping excitations,

$$\Psi_{M_s=0}^{s,t} = \hat{R}_{M_s=-1} \tilde{\Psi}_{M_s=+1}^t, \quad (2)$$

where $\tilde{\Psi}_{M_s=+1}^t$ is the $\alpha\alpha$ component of the triplet reference state, $\Psi_{M_s=0}^{s,t}$ stands for the final ($M_s = 0$) singlet and triplet states, respectively, and the operator $\hat{R}_{M_s=-1}$ is an excitation operator that flips the spin of an electron. Likewise, (multi-configurational) doublet and quartet states can be described by applying spin-flipping ($M_s = -1$) operator to the high-spin quartet reference. As can be seen from Fig. 2, the determinants generated in this way include all configurations necessary for describing ground and excited states of diradicals (top) and triradicals (bottom). Note that only the leading configurations, i.e., those corresponding to two-electrons-in-two-orbitals in diradicals and three-electrons-in-three-orbitals

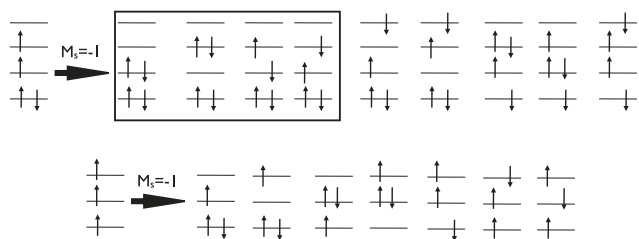


FIG. 2. Target determinants generated by a spin-flipping ($M_s = -1$) excitation operator from a triplet (top) or a quartet (bottom) reference in the CIS or TD-DFT/TDA methods. In the top panel, the box includes configurations forming proper target SF states.

in triradicals, form a spin-complete set, whereas some determinants derived by excitations that change the number of electrons in the open-shell subspace miss some of their spin-counterparts. This may lead to a slight spin-contamination of the proper SF states (e.g., lowest diradical states dominated by the configurations derived from two-electrons-in-two-orbitals set), or a large spin-contamination of other states that involve excitations outside the open-shell subspace. In the wave function based formulation it can be easily remedied either by including a well-defined selected set of determinants¹⁷ or by removing the determinants that do not have their counterparts.¹⁸ The spin-symmetry of the target SF-TDDFT states is a more complicated issue and is discussed below.

When implemented within EOM-CCSD framework, the resulting EOM-SF-CCSD method provides robust and accurate tool for dealing with electronic wave functions that can be described, in a multi-reference jargon, as two-electron-in-two-orbitals or three-electrons-in-three-orbitals type, as illustrated by numerous applications and benchmark studies.^{19,20} The EOM-SF-CCSD can be augmented by perturbative triples corrections²¹ or explicit inclusion of triples,²² which allows one to compute relevant energetics (e.g., singlet-triplet (ST) or doublet-quartet gaps) with chemical accuracy.

While the EOM-SF-CCSD method is robust and accurate, its applications are limited to moderate-size systems due to the N^6 scaling of the underlying CCSD calculation. The SF-TDDFT approach^{23–29} is an attractive alternative to EOM-SF-CCSD that extends DFT to systems with extensive electronic degeneracies, such as diradicals, triradicals, and even transition metals. Since its introduction²⁴ in 2003, the SF-TDDFT method has been applied to a variety of interesting systems (more than 100 citations).

Just as in the wave function based methods, the target states in SF-TDDFT are described as spin-flipping ($M_s = -1$) “excitations” from a well-behaved high-spin (e.g., $M_s = 1$) reference state. For example, as illustrated in Fig. 3, all leading determinants in the low-lying states of methylene are single spin-flipping excitations from the high-spin triplet reference $|a_1\alpha b_1\alpha\rangle$:

$$X^3 B_1 \sim |a_1\alpha b_1\beta\rangle + |a_1\beta b_1\alpha\rangle, \quad (3)$$

$$\tilde{b}^1 B_1 \sim |a_1\alpha b_1\beta\rangle - |a_1\beta b_1\alpha\rangle, \quad (4)$$

$$\tilde{a}^1 A_1 \sim |a_1\alpha a_1\beta\rangle - \lambda |b_1\alpha b_1\beta\rangle, \quad (5)$$

$$\tilde{c}^1 A_1 \sim \lambda |a_1\alpha a_1\beta\rangle + |b_1\alpha b_1\beta\rangle. \quad (6)$$

Contrary to the spin-symmetry broken DFT approach, the target SF wave functions do not involve unphysical scrambling of triplet and singlet states, or mixing of open- and closed-shell singlets. Note that SF-TDDFT distinguishes between two different types of singlet diradicals, i.e., open- and closed-shell types such as $\tilde{b}^1 B_1$ and $\tilde{a}^1 A_1$ states of methylene, whereas spin-projected spin-symmetry broken DFT will treat these two states as identical. Since different singlet states have different character (e.g., various degrees of ionic versus

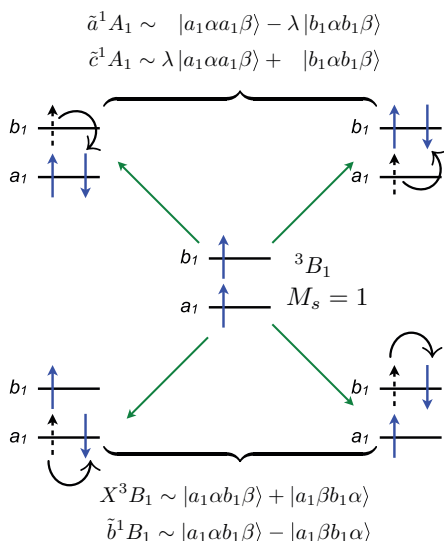


FIG. 3. Electronic configurations of the low-lying states of methylene and the high-spin reference.

covalent contributions), such scrambling is unphysical. Moreover, it cannot be cleaned up by spin-projection.

The issue of spin-purity in DFT is more complicated than in the wave function based formalism. Strictly speaking, the expectation value of the \hat{S}^2 operator cannot be determined from the KS density alone (and even less so from the TD-DFT amplitudes), as it is a two-electron operator. Thus, $\langle S^2 \rangle$ of the KS determinant does not represent the degree of spin-contamination of the (unknown) wave function giving rise to that density. Furthermore, for open-shell species the density derived from the exact wave function must be slightly spin-polarized and cannot be represented by a restricted open-shell Hartree-Fock (ROHF) KS determinant (e.g., for a doublet $M_s = \frac{1}{2}$ radical, there should be areas of an excess β density which cannot be reproduced by ROHF).³⁰ On these grounds, Pople, Gill, and Handy have advocated that the ROHF formulation of KS theory should be avoided.³⁰ However, the bulk of computational experience suggests that large spin-contamination (e.g., $\langle S^2 \rangle$ values around 1 for even number of electrons) of the KS or TDDFT “wave functions” is indicative of a problematic behavior justifying some degree of spin-adaptation.

In the context of SF-TDDFT, there are two sources of spin-contamination, that is, due to using spin-unrestricted KS reference and due to spin-incompleteness of a strictly singly excited set of determinants generated from an open-shell reference. As discussed before,^{17,18,23} one should distinguish between “proper” SF target states (those whose wave functions are dominated by configurations derived by excitations within singly occupied space, such as those enclosed in the box in Fig. 2(a) or in Fig. 2(b)) and higher excited states dominated by excitations either from doubly occupied orbitals or to unoccupied orbitals. For the former group, the SF set of determinants includes all necessary leading configurations; thus, $\langle S^2 \rangle$ for these states are usually very close to spin-pure values (e.g., typical values observed in this study are 0.01–0.2 for the singlets and 2.01–2.2 for the triplets). Larger deviations may

occur if the high-spin reference is strongly spin-contaminated (e.g., we observed deviations as large as 0.4 in *meta*-xylylene (MX)); in such cases using the ROHF-based formulation may be justified. Furthermore, these primary SF states can be strictly spin-adapted by discarding some of the open-shell SF determinants that do not have their spin-adapted counterparts, as was done in the CIS implementation.¹⁸ For the second group of states, the SF set is not spin-complete and we often observe unphysical $\langle S^2 \rangle$ values (~ 1). As discussed by Rinkevicius and co-workers, one may consider using fully spin-adapted SF operator to improve their description,²³ similarly to the implementation discussed in Ref. 17, which will require inclusion of selected higher excitations^{17,18} that can only be justified beyond adiabatic approximation. One possible solution was suggested by Li and Liu through a tensor reference.^{31–33} Such fully spin-adapted SF-TDDFT variants might be useful for describing higher excited states in diradicals and triradicals (as well as more problematic diradicals such as oxygen-containing ones that have a four-electrons-in-three-orbitals type of electronic structure) further extending the applicability of the SF method.

The original implementation²⁴ of SF-TDDFT was based on the so-called collinear formalism in which the SF states can only be coupled by the Hartree-Fock exchange operator. This limited the applications of the method to hybrid functionals and required relatively large fractions of HF exchange (about 50%). The performance of the method for most diradicals and triradicals (both structures and energetics) is quite remarkable, e.g., SF-TDDFT/50-50 energy gaps are within 1-3 kcal/mol from the experimental or SF-CCSD values; however, a number of surprising failures, all involving small diradicals, was noted.²⁴

Later, Ziegler’s group^{26,27} reformulated SF-TDDFT using non-collinear exchange-correlation (XC) kernels, i.e., those that formally allow mixing of α and β orbitals. These non-collinear XC kernels were first proposed by Liu and co-workers in the context of relativistic TD-DFT.^{34,35} While Ziegler’s implementation is based on the normal KS reference equations and collapses to regular TD-DFT for non-spin-flipping excitations, it cleverly allows one to introduce coupling between the spin-flip target configurations with local functionals. Thus, it extends SF to “pure” functionals, such as local density or generalized gradient approximations (LDA or GGA). In addition to an aesthetic formal appeal, Ziegler’s benchmarks²⁶ for atoms and small diradicals (NH_2^+ , CH_2 , SiH_2) yielded better results than original SF-TDDFT/50-50.

Original and non-collinear SF-TDDFT have been implemented in several electronic structure packages and applied to problems involving diradicals,^{36,37} triradicals^{20,38–41} as well as conical intersections such as *cis-trans* isomerization around a double bond and ring opening in oxirane.^{28,42,43} The authors of the SF-TDDFT stilbene study⁴³ have noted a superior performance of SF-TDDFT relative to 2×2 CASPT2, which, we believe, is due to a balanced treatment of dynamical and non-dynamical correlation by the SF-TDDFT ansatz. Finally, Rinkevicius and co-workers extended non-collinear SF-TDDFT to work with hybrid functionals improving the accuracy even further.²³ They reported impressive results

for a variety aromatic diradicals²⁹ and for excited states in polyenes²³ using BHHLYP. While the implementations from Rinkevicius and co-workers²³ considered TDA variants of SF-TDDFT, Li and Liu recently reported full SF-TDDFT results⁴⁴ and assessed the performance of several SF-TDDFT models with selected functionals for bond-breaking, excited states in doublet radicals and closed-shell molecules. They noted that the TDA formulation is more appropriate for SF applications as RPA might be affected by the reference instabilities and also might become problematic for states with negative “excitation” energies.

This paper reports a general implementation of non-collinear SF-TDDFT in the *Q-Chem* software package.⁴⁵ We implemented both energies and analytic gradients for LDA, GGA, hybrid, and long-range corrected (LRC) functionals. Technically, our implementation is very similar to that of Rinkevicius and co-workers^{23,29} that includes both HF exchange coupling terms (which are part of the collinear SF-TDDFT equations²⁴) and the non-collinear coupling terms of Ziegler and Wang.²⁶ In this paper, we employ the TDA variant (both energies and analytic gradients) and present an extensive benchmark study using a wide variety of functionals.

II. THEORY OF SF-TDDFT

A. TD-DFT/TDA

Within TD-DFT/TDA, excited states are described as one-electron excitations (Φ_i^a) from occupied spin-orbitals (i, j, \dots) of the reference KS ground-state determinant (Φ_0) into virtual spin-orbitals (a, b, \dots), and the excitation amplitudes ($\mathbf{X} = \{X_i^a\}$) satisfy the TD-DFT/TDA eigen-equation,

$$\mathbf{A}\mathbf{X} = \omega\mathbf{X}, \quad (7)$$

where ω is the excitation energy. The coupling matrix, \mathbf{A} , contains a one-electron term and the response of the KS Fock matrix (\mathbf{F}) with respect to a perturbation in the one-particle density matrix (\mathbf{P}),

$$\begin{aligned} \mathbf{A}_{ai,bj} &= (\epsilon_a - \epsilon_i)\delta_{ab}\delta_{ij} + \frac{\partial \mathbf{F}_{ai}}{\partial \mathbf{P}^{bj}} \\ &= (\epsilon_a - \epsilon_i)\delta_{ab}\delta_{ij} + (ia|jb) - C_{HF}(ij|ab) + (ia|\varpi|jb), \end{aligned} \quad (8)$$

which includes contributions from: (i) the KS orbital energies (ϵ_a and ϵ_i), (ii) two-electron repulsion integrals of the Coulomb-type, $(ia|jb)$, and the exchange-type, $(ij|ab)$, with the following spatial part:

$$(ia|jb) = \int \psi_i(\mathbf{r})\psi_a(\mathbf{r}) \frac{1}{|\mathbf{r} - \mathbf{r}'|} \psi_j(\mathbf{r}')\psi_b(\mathbf{r}') d\mathbf{r}d\mathbf{r}', \quad (9)$$

$$(ij|ab) = \int \psi_i(\mathbf{r})\psi_j(\mathbf{r}) \frac{1}{|\mathbf{r} - \mathbf{r}'|} \psi_a(\mathbf{r}')\psi_b(\mathbf{r}') d\mathbf{r}d\mathbf{r}'; \quad (10)$$

and (iii) the response in the KS exchange-correlation matrix, $(ia|\varpi|jb)$,

$$(ia|\varpi|jb) = \frac{\partial \mathbf{F}_{xc,ai}}{\partial \mathbf{P}^{bj}}. \quad (11)$$

The coefficient C_{HF} in Eq. (8) comes from the fraction of Hartree-Fock exchange in a given exchange-correlation energy functional.

B. SF-TDDFT with a collinear kernel

In SF-TDDFT, TD-DFT/TDA is solved within the subspace of spin-flipped determinants from the lowest energy triplet ($M_s = 1$), which is used as the reference KS state for a system with an even number of electrons, as illustrated in Fig. 2. The target set of determinants is generated by exciting a single electron from α occupied orbitals ($i, j \in \alpha$) into β virtual orbitals ($a, b \in \beta$); these determinants form a balanced basis for representing the lowest energy singlet states and the $M_s = 0$ component of the lowest energy triplet state. In the original SF-TDDFT,²⁴ a standard collinear kernel is applied in the evaluation of matrix \mathbf{A} in Eq. (8). Since a change in the $\beta\alpha$ -block of the density ($\delta \mathbf{P}^{bj}$) does not affect the α and β electronic densities or their gradients, there is no response in either the Coulomb potential or the exchange-correlation potential. As a result, the second and fourth terms in Eq. (8) vanish,

$$(ia|jb) = 0, \quad (ia|\varpi|jb) = 0, \quad i, j \in \alpha \text{ and } a, b \in \beta, \quad (12)$$

leaving different spin-flip excitations coupled only through the Hartree-Fock exact exchange, $-C_{HF}(ij|ab)$, which is the third term in Eq. (8).

C. SF-TDDFT with non-collinear kernel

In the Wang-Ziegler formulation of SF-TDDFT,^{25,26,46} the exchange-correlation kernel is replaced with a non-collinear kernel,

$$\begin{aligned} (ia|\varpi|jb) &\rightarrow \int \psi_a(\mathbf{r})\psi_i(\mathbf{r}) \frac{1}{\rho_\alpha - \rho_\beta} \\ &\times \left(\frac{\delta E^{xc}}{\delta \rho_\alpha} - \frac{\delta E^{xc}}{\delta \rho_\beta} \right) \psi_b(\mathbf{r})\psi_j(\mathbf{r}) d\mathbf{r}. \end{aligned} \quad (13)$$

The excitation energy for non-collinear SF-TDDFT/TDA has the same energy expression as conventional TD-DFT/TDA,⁴⁷

$$\omega = \mathbf{X}^\dagger \cdot \mathbf{A} \cdot \mathbf{X} = \mathbf{F} \cdot \mathbf{P}_\omega + \mathbf{R}_\omega^\dagger \cdot \mathbf{\Pi} \cdot \mathbf{R}_\omega + \mathbf{R}_\omega^\dagger \cdot \mathbf{\Omega} \cdot \mathbf{R}_\omega, \quad (14)$$

where $\mathbf{\Pi}$ denotes two-electron integrals and \mathbf{P}_ω is the unrelaxed difference density matrix,

$$\mathbf{P}_\omega = \mathbf{C}_v^\beta \mathbf{X} \mathbf{X}^\dagger \mathbf{C}_v^{\beta\dagger} - \mathbf{C}_o^\alpha \mathbf{X}^\dagger \mathbf{X} \mathbf{C}_o^{\alpha\dagger}. \quad (15)$$

The dimension of the excitation amplitude matrix, \mathbf{X} , is v_β (number of β virtual orbitals) times o_α (number of α occupied orbitals), and matrix \mathbf{C}_o (\mathbf{C}_v) gives coefficients of the KS occupied (virtual) molecular orbitals in terms of atomic basis functions, with the dimension being $N \times o$ ($N \times v$), where N is the number of atomic basis functions. Thus, the first term in Eq. (15) reflects a net gain in the β -space electron density and the second term is a net decrease in the α -space. The transition density matrix in Eq. (14) is

$$\mathbf{R}_\omega = \mathbf{C}_v^\beta \mathbf{X} \mathbf{C}_o^{\alpha\dagger}. \quad (16)$$

For standard TD-DFT/TDA, the last term in Eq. (14) is

$$\Omega_{\mu\nu,\lambda\sigma} = \frac{\partial \mathbf{F}_{xc,\mu\nu}}{\partial \mathbf{P}^{\lambda\sigma}} = \int \sum_{\xi,\xi'} \frac{\partial^2 f_{xc}}{\partial \xi \partial \xi'} \frac{\partial \xi}{\partial P^{\mu\nu}} \frac{\partial \xi'}{\partial P^{\lambda\sigma}} d\mathbf{r}, \quad (17)$$

where $\mu, \nu, \lambda, \sigma$ denote atomic basis functions, ξ and ξ' refer to independent variables such as density (ρ_α, ρ_β) and their first derivatives ($\rho_\alpha^x, \rho_\alpha^y, \rho_\alpha^z, \rho_\beta^x, \rho_\beta^y, \rho_\beta^z$).

For non-collinear SF-TDA, the functional second derivatives are replaced with the non-collinear kernel in Eq. (13),

$$\frac{\partial^2 f_{xc}}{\partial \xi \partial \xi'} \rightarrow \frac{1}{\rho_\alpha - \rho_\beta} \left(\frac{\delta E^{xc}}{\delta \rho_\alpha} - \frac{\delta E^{xc}}{\delta \rho_\beta} \right), \text{ if } \xi = \xi' = \rho_\alpha$$

0, otherwise. (18)

As noted before,^{23,44} the denominators involving the spin-density ($\rho_\alpha - \rho_\beta$) that appear in the non-collinear GGA kernels in Eq. (18) may lead to numeric instabilities. Thus, a tighter grid is usually required for non-collinear SF-TDDFT with GGA. In energy calculations, we observed stable behavior with the SG-1(50,194) grid, e.g., the results with the (100, 302) grid were very similar to the SG-1 ones. In the case of analytic gradient calculations, which are more sensitive to these instabilities, using tighter grids does not help. Li and Liu⁴⁴ proposed a simple approximation (called ALDA0) that removes most problematic terms. Their benchmarks indicate that errors introduced by ALDA0 are about 0.15 eV. As the numerical instabilities are more severe in the analytical gradient calculations (see Appendix A), which in our implementation makes geometry optimization feasible only with the LDA functional.

III. COMPUTATIONAL DETAILS

To calibrate the performance of SF-TDDFT with different functionals, we consider the following benchmark sets:

1. Multiplet separation (ST and doublet-quartet gaps) in atomic systems (C, N, O, Si, P, and S).
2. Adiabatic energy gaps between the lowest electronic states ($^3B_1, 1^1A_1, 1^1B_1$, and 2^1A_1) in carbene-like diradicals ($\text{CH}_2, \text{NH}_2^+, \text{SiH}_2$, and PH_2^+).
3. Vertical energy gaps between the lowest electronic states in diradicals derived by the ring opening in cyclohexane and methyl-cyclohexane (two types of diradicals are considered—carbene-like and 1,6 ones, with unpaired electrons on different ends of the molecule, see Fig. 4).
4. Adiabatic energy gaps between the electronic states ($^3B_1, 1^1B_1, 1^1A_1$, and 2^1A_1) in trimethylmethane (TMM), see Fig. 5.
5. Adiabatic ST gaps in $\sigma\sigma, \sigma\pi$, and $\pi\pi$ diradicals (benzynes, didehydrotoluenes (DHT), and MX, see Fig. 5).

The mean average deviation (MAD) is computed versus EOM-SF-CCSD(dT)²¹ values calculated with at least the 6-311G(d) basis (cyclohexane and methyl-cyclohexane diradicals). Much larger basis sets were used in atoms and in small diradicals (aug-cc-pVQZ). For all other diradicals, the cc-pVTZ basis was used. The EOM-SF-CCSD(dT) method, which includes perturbative triples correction, has been cali-

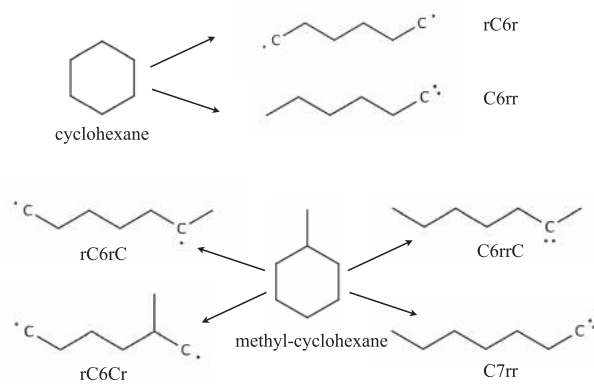


FIG. 4. Structures of diradicals derived by the ring opening in cyclohexane and methyl-cyclohexane. The unpaired electrons are denoted by “r,” e.g., rC6r is a 1,6 diradical, whereas C6rr is a carbene-like diradical.

brated against available experimental values for selected diradicals and was shown to further improve the accuracy of EOM-SF-CCSD.¹⁹ We estimate the error bars for this method to be below 1 kcal/mol (chemical accuracy). Unrestricted triplet references were used in most coupled-cluster calculations, except for selected cases with large reference spin-contamination. The details of the EOM-SF-CCSD and EOM-SF-CCSD(dT) calculations for each system are summarized in the supplementary material.⁴⁸

For molecular systems, we compute adiabatic gaps using the same geometries for all methods (i.e., the best available equilibrium geometries for the singlet and triplet states of a given diradical) in order to eliminate the uncertainties due to different structures and focus on energy differences only. We assess the quality of optimized structures separately. We focus on electronic energy differences and do not include zero-point energy corrections. We used the same geometries as in previous benchmark studies when possible. For carbene-like diradicals and TMM, the same equilibrium geometries as in the previous benchmark study,¹⁹ i.e., full configuration interaction (FCI)/TZ2P optimized geometries⁴⁹ for CH_2 , and CISD/TZ2P(f,d) optimized geometries for NH_2^+ , SiH_2 , and PH_2^+ (Refs. 50–52), and SF-TDDFT/50-50/6-311G(d) for TMM.

For benzynes, we employed SF-TDDFT/50-50/6-311G(d) geometry from Ref. 14. For didehydrotoluenes, we

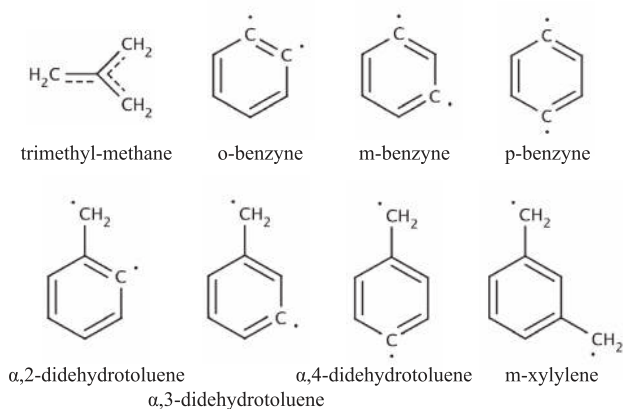


FIG. 5. Structures of selected diradicals.

computed SF-TDDFT/50-50/6-311G(d) optimized geometries. For MX, we employed CCSD and SF-CCSD optimized geometries using 6-31G(d) from Ref. 53.

For diradicals derived from cyclohexane/methylcyclohexane, vertical state differences were computed at the optimized singlet B3LYP/6-311G(2d,p) geometries (C6rr, C7rr, rC6Cr), except for rC6r for which an optimized triplet geometry was used.

All Cartesian coordinates and relevant energies are collected in the supplementary material.⁴⁸

All SF-TDDFT calculations were performed with the cc-pVTZ basis set. We found that SF-TDDFT is not very sensitive to the basis set, and that the 6-311G(d) results are almost as good as the cc-pVTZ ones. However, 6-31G(d) is too small.

We tested NC-SF-TDDFT with the following functionals: (i) LDA (Slater exchange and VWN correlation); (ii) Becke-exchange/LYP correlation family: BLYP,^{54,55} B3LYP,^{56,57} 50-50 (50% Hartree-Fock + 8% Slater + 42% Becke for exchange and 19% VWN + 81% LYP for correlation), and BHHLYP (50% Hartree-Fock + 50% Becke for exchange and 100% LYP for correlation); (iii) B97 family: B97, ω B97, and ω B97X (Refs. 58 and 59); (iv) P86 correlation with Becke exchange: BP86, B3P86 (Refs. 54 and 60); (v) PW91: PW91, B3PW91 (Refs. 61–64); (vi) PBE family: PBE, PBE0 (75% PBE and 25% Hartree-Fock exchange, 100% PBE correlation), PBE50 (50% PBE and 50% Hartree-Fock exchange and 100% PBE correlation), and ω PBEh (80% PBE, 20% Hartree-Fock exchange and long-range Hartree-Fock exchange, 100% PBE correlation^{65,66}). We also provide results for collinear SF-TDDFT with the 50-50 functional, which was recommended in the original SF-TDDFT paper,²⁴ and for the PBE50 functional for comparison.

This selection allows us to assess relative performance of different exchange and correlation functionals in the context of SF-TDDFT. The most general comparisons are between LDA and GGA (e.g., LDA versus PW91, PBE, BP86), between GGAs and hybrids (e.g., BLYP versus B3LYP, PBE versus PBE0 versus PBE50, BP86 versus B3P86), and between GGAs and LRCs (B97 versus ω B97/ ω B97X, PBE0 versus ω PBEh). In addition, we can compare functionals that have same exchange but different correlation, and vice versa,

e.g., BLYP versus BP86, B3LYP versus B3PW91 versus B3P86, PBE versus PW91, and B3PW91 versus PBE0 (those differ by exchange).

To benchmark the performance of SF-TDDFT for equilibrium geometries, we considered structures of benzynes optimized using non-collinear SF-TDDFT/LDA and the cc-pVTZ basis and compared them against the SF-CCSD/cc-pVTZ and collinear SF-TDDFT/50-50/6-311G(d) values.²⁴

For excitation energy calculations, the default grid in *Q-Chem*, SG-1(50,194), was found to be sufficient (the SG-0 grid is too small). For analytical gradient, a bigger grid such as (150,302) is necessary.

We employ unrestricted KS references. In some cases, we note that hybrid GGA functionals lead to a large spin-contamination in the reference triplet (and, consequently, in the target states).

IV. RESULTS AND DISCUSSION

A. Energetics

Figure 6 presents MAD for 22 ST gaps for the following systems: C, O, Si, S, CH₂, NH₂⁺, SiH₂, PH₂⁺, TMM, hexane family (C6rr, C7rr, C6rrC, rC6r, rC6Cr, rC6rC, see Fig. 4), *ortho*-, *meta*-, and *para*-benzynes, α 2-, α 3-, and α 4-didehydrotoluenes, and *meta*-xylylene. Figure 7 presents MAD computed for a larger set of states (41) which, in addition to the lowest singlet and triplet, also includes other low-lying states. The respective data are summarized in Tables I–VI. For rC6r, rC6rC, and rC6Cr, only the ST gaps were included in MAD calculation, as the errors of higher excited states are too large due to their strongly ionic character; the errors for these states are analyzed separately.

As we can see from Figs. 6 and 7, SF-CCSD is very close to the reference SF-CCSD(dT) values, as expected based on earlier benchmark study that compared the performance of SF-CCSD against available experimental values.¹⁹ The MAD of original (collinear) SF-TDDFT/50-50 is about 0.35 eV (see Fig. 7). Using another exchange-correlation (with the same fraction of HF exchange) in the collinear SF-TDDFT

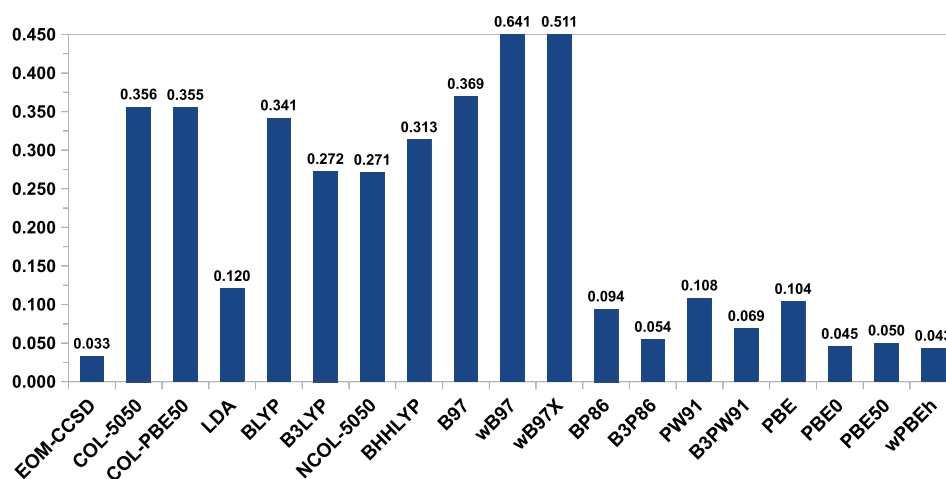


FIG. 6. MAD (eV) of 22 singlet-triplet gaps.

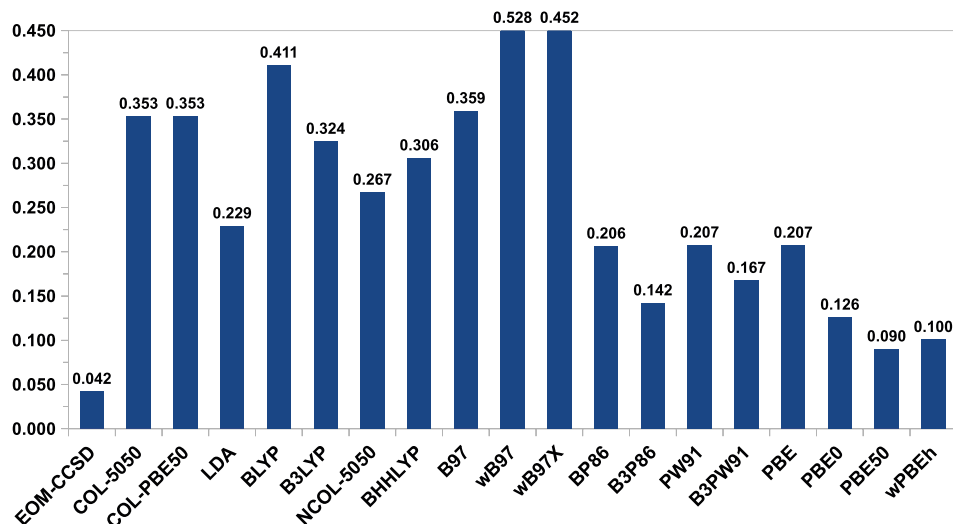


FIG. 7. MAD (eV) for 41 gaps between low-lying electronic states in various atomic and molecular systems.

does not improve the accuracy, i.e., collinear SF-TDDFT with PBE50 has the same MAD. The analysis of the data in Tables I–VI reveals that large MAD of collinear SF-TDDFT is due to large errors in atoms and same-center diradicals (carbene-like), whereas MAD in all other diradicals is much smaller (~ 0.1 eV).

Non-collinear SF-TDDFT/50-50 shows only a moderate improvement over collinear SF-TDDFT. We note consistently poor performance of all functionals that include LYP correlation: BLYP, B3LYP, 50-50, and BHLYP. Notably, 50-50 that includes only 81% of LYP performs slightly better than BHLYP. Comparing BLYP with BP86 (or B3LYP with

B3PW91 or B3P86), we observe that errors are reduced by almost a factor of two. The performance of B97, ω B97, and ω B97X is rather disappointing, especially in view of excellent performance of ω B97X for a variety of thermochemical properties.⁵⁹ These GGA functionals are based on LDA correlation (PW92⁶²) and treat the correlation of same-spin and different-spin electrons differently using the so-called Stoll trick^{67,68} to account for the fact that in the finite systems the correlation between same-spin electrons is smaller than between the opposite-spin electrons, contrary to the uniform electron gas. This correction might affect the performance of these functionals in SF calculations that involve changing

TABLE I. Total ground-state energies (hartree) and multiplet gaps (eV) in selected atoms.

	C		N		O		Si		P		S		MAD All
	3P	1D	4S	2D	3P	1D	3P	1D	4S	2D	3P	1D	
CCSD(dT) ^a	-37.81958	1.271	-54.56246	2.402	-75.03624	1.972	-289.10647	0.766	-341.00361	1.427	-397.84727	1.138	-
CCSD ^a	-37.81789	1.249	-54.56051	2.380	-75.03393	1.963	-289.10359	0.733	-340.99995	1.381	-397.84282	1.111	0.027
C-5050	-37.80392	0.727	-54.53093	1.334	-74.99836	1.063	-289.33114	0.479	-341.21542	0.852	-398.05597	0.664	0.643
C-PBE50	-37.76671	0.731	-54.48824	1.342	-74.94907	1.067	-289.25360	0.485	-341.13790	0.863	-397.97670	0.670	0.636
LDA	-37.46605	1.346	-54.13041	2.429	-74.51997	1.885	-288.21084	0.723	-339.99451	1.258	-396.73195	0.950	0.098
BLYP	-37.81796	0.985	-54.56110	1.831	-75.04244	1.544	-289.36468	0.534	-341.25185	0.928	-398.09924	0.741	0.402
B3LYP	-37.83577	0.982	-54.57987	1.848	-75.06100	1.556	-289.38273	0.533	-341.27193	0.955	-398.11991	0.771	0.388
NC-5050	-37.81549	0.889	-54.55389	1.720	-75.02935	1.490	-289.33065	0.475	-341.21802	0.893	-398.06345	0.756	0.459
BHLYP	-37.81924	0.821	-54.55890	1.603	-75.03789	1.417	-289.36534	0.437	-341.25585	0.826	-398.10581	0.710	0.527
B97	-37.81887	1.017	-54.56352	2.039	-75.04447	1.779	-289.30343	0.354	-341.19036	0.803	-398.04257	0.745	0.373
ωB97	-37.80816	0.705	-54.55797	1.767	-75.05203	1.784	-289.31136	-0.033	-341.20201	0.225	-398.07449	0.457	0.679
ωB97X	-37.80971	0.890	-54.55792	1.965	-75.04828	1.792	-289.31857	-0.025	-341.20990	0.314	-398.08083	0.504	0.589
BP86	-37.84164	1.398	-54.59674	2.549	-75.07033	2.013	-289.39792	0.801	-341.30111	1.393	-398.15042	1.052	0.078
B3P86	-37.83389	1.321	-54.58403	2.437	-75.05461	1.949	-289.35700	0.747	-341.25542	1.329	-398.10091	1.028	0.056
PW91	-37.81727	1.378	-54.57044	2.521	-75.04166	1.990	-289.34517	0.759	-341.24487	1.344	-398.09198	1.023	0.075
B3PW91	-37.83274	1.386	-54.58346	2.535	-75.05111	2.008	-289.34000	0.821	-341.23742	1.431	-398.07876	1.086	0.066
PBE	-37.78571	1.374	-54.52953	2.518	-74.98996	2.002	-289.21687	0.796	-341.10266	1.394	-397.93349	1.059	0.065
PBE0	-37.79673	1.320	-54.54123	2.447	-75.00180	1.969	-289.24593	0.771	-341.13669	1.374	-397.97103	1.061	0.039
PBE50	-37.80832	1.261	-54.55356	2.368	-75.01462	1.929	-289.27591	0.742	-341.17152	1.345	-398.00975	1.061	0.045
ωPBEh	-37.80196	1.302	-54.54641	2.430	-75.00777	1.967	-289.25058	0.745	-341.14134	1.342	-397.97626	1.049	0.043
Expt. ^b		1.264		2.384		1.967		0.781		1.409		1.145	

^aaug-cc-pV5Z basis set.^bReference 70.

TABLE II. Total ground-state energies (hartree) and adiabatic excitation energies (eV) for the three lowest states of CH₂, NH₂⁺, SiH₂, PH₂⁺.

	CH ₂				NH ₂ ⁺				SiH ₂				PH ₂ ⁺				MAD		
	³ B ₁	¹ A ₁	¹ B ₁	¹ A ₁	³ B ₁	¹ A ₁	¹ B ₁	¹ A ₁	¹ A ₁	³ B ₁	¹ B ₁	¹ A ₁	¹ A ₁	³ B ₁	¹ B ₁	¹ A ₁	S-T	S-S ^a	All
(dT) ^b	-39.11427	0.420	1.410	2.530	-55.42944	1.253	1.865	3.318	-290.22664	0.892	1.937	3.365	-341.76279	0.794	1.993	3.640	-	-	-
CCSD ^b	-39.11206	0.447	1.432	2.583	-55.42736	1.273	1.884	3.362	-290.22378	0.874	1.950	3.425	-341.75955	0.778	1.995	3.691	0.020	0.005	0.029
C-5050	-39.10937	-0.249	0.858	1.711	-55.40537	0.255	1.016	2.045	-290.59016	1.307	2.116	3.438	-342.12000	1.318	2.163	3.593	0.652	0.154	0.547
C-PBE50	-39.07296	-0.216	0.855	1.697	-55.36476	0.298	1.012	2.039	-290.51409	1.278	2.076	3.391	-342.04212	1.301	2.136	3.558	0.621	0.116	0.533
LDA	-38.76069	0.511	1.331	2.677	-54.99688	1.284	1.769	3.523	-289.43485	0.934	1.759	3.207	-340.86466	0.836	1.808	3.388	0.051	0.165	0.125
BLYP	-39.10966	-0.013	0.957	1.931	-55.42802	0.716	1.377	2.689	-290.61213	1.355	1.963	3.254	-342.15049	1.335	2.040	3.422	0.493	0.035	0.379
B3LYP	-39.14123	0.019	1.005	1.998	-55.45381	0.749	1.381	2.729	-290.64236	1.306	2.011	3.327	-342.17504	1.268	2.066	3.503	0.448	0.046	0.344
NC-5050	-39.11618	-0.112	0.961	1.896	-55.42512	0.627	1.285	2.583	-290.58904	1.358	2.129	3.414	-342.12024	1.301	2.153	3.600	0.532	0.120	0.414
BHHLYP	-39.11402	-0.213	0.690	1.734	-55.42774	0.529	1.214	2.416	-290.62089	1.426	2.151	3.392	-342.15827	1.385	2.178	3.566	0.621	0.140	0.504
B97	-39.11483	-0.394	0.872	1.720	-55.44133	0.807	1.536	2.957	-290.57710	1.886	2.150	3.152	-342.10669	1.593	2.154	3.406	0.763	0.192	0.493
ωB97	-39.10461	-1.084	0.537	1.073	-55.43822	0.456	1.387	2.609	-290.61263	2.675	2.429	3.222	-342.14777	2.352	2.387	3.250	1.410	0.459	0.882
ωB97X	-39.10398	-0.702	0.683	1.208	-55.43749	0.801	1.499	2.794	-290.61031	2.585	2.298	3.080	-342.14547	2.124	2.289	3.181	1.149	0.284	0.745
BP86	-39.15019	0.662	1.454	2.922	-55.46806	1.429	1.919	3.808	-290.64358	0.866	1.814	3.419	-342.18465	0.761	1.874	3.655	0.119	0.141	0.147
B3P86	-39.14636	0.561	1.417	2.824	-55.45859	1.348	1.847	3.683	-290.60883	0.915	1.870	3.469	-342.14277	0.798	1.931	3.702	0.066	0.094	0.103
PW91	-39.11996	0.498	1.371	2.725	-55.43877	1.349	1.866	3.685	-290.59001	1.001	1.851	3.340	-342.12860	0.865	1.896	3.582	0.088	0.099	0.102
B3PW91	-39.14394	0.683	1.511	3.014	-55.45700	1.448	1.925	3.840	-290.58657	0.809	1.875	3.570	-342.12098	0.703	1.913	3.779	0.158	0.110	0.190
PBE	-39.08553	0.534	1.400	2.813	-55.39623	1.356	1.877	3.732	-290.45615	0.962	1.843	3.399	-341.98231	0.823	1.887	3.626	0.079	0.104	0.107
PBE0	-39.09955	0.507	1.410	2.820	-55.40999	1.336	1.856	3.701	-290.48887	0.944	1.918	3.507	-342.01753	0.800	1.943	3.784	0.057	0.062	0.106
PBE50	-39.11495	0.478	1.423	2.838	-55.42475	1.301	1.826	3.671	-290.52360	0.922	2.003	3.617	-342.05474	0.777	2.006	3.860	0.038	0.053	0.118
ωPBEh	-39.10971	0.526	1.417	2.820	-55.41773	1.342	1.850	3.692	-290.49727	0.929	1.925	3.513	-342.02380	0.784	1.931	3.722	0.061	0.070	0.103
Expt. ^c		0.390	1.425			1.306				0.91	1.928			0.75	1.92				

^a¹A₁ - ¹B₁.^baug-cc-pVQZ basis set.^cFrom Ref. 19.

TABLE III. Total ground-state energies (hartree) and vertical excitation energies (eV) of 3 diradicals (unpaired electrons on the same center) from the ring opening of cyclohexane and methylcyclohexane.

	C6rr				C7rr				C6rrC				MAD		
	1A_1	3B_1	1B_1	1A_1	1A_1	3B_1	1B_1	1A_1	1A_1	3B_1	1B_1	1A_1	S-T	S-S	All
(dT) ^a	-234.99342	0.614	2.365	5.545	-274.18522	0.623	2.374	5.558	-274.20139	0.696	2.377	5.546	-	-	-
CCSD ^a	-234.99035	0.587	2.373	5.601	-274.18217	0.596	2.382	5.616	-274.19742	0.661	2.387	5.607	0.030	0.034	0.032
C-5050	-235.63485	1.396	2.391	5.369	-274.93410	1.404	2.400	5.379	-274.95027	1.446	2.412	5.396	0.771	0.099	0.323
C-PBE50	-235.53981	1.361	2.356	5.329	-274.82703	1.370	2.364	5.342	-274.84417	1.411	2.371	5.306	0.736	0.116	0.323
LDA	-233.55393	0.781	2.020	4.970	-272.50988	0.789	2.028	4.920	-272.53090	0.922	2.101	4.973	0.186	0.459	0.368
BLYP	-235.64535	1.223	2.145	4.964	-274.94608	1.231	2.154	4.975	-274.96535	1.299	2.180	4.997	0.607	0.392	0.463
B3LYP	-235.80608	1.160	2.209	5.135	-275.13392	1.168	2.213	5.151	-275.15195	1.223	2.234	5.145	0.539	0.280	0.366
NC-5050	-235.63712	1.235	2.350	5.374	-274.93635	1.244	2.358	5.450	-274.95274	1.268	2.359	5.416	0.605	0.076	0.253
BHHLYP	-235.64612	1.329	2.376	5.370	-274.94686	1.336	2.370	5.427	-274.96319	1.355	2.376	5.401	0.696	0.078	0.284
B97	-235.71662	1.379	2.330	5.216	-275.02947	1.390	2.335	5.235	-275.04686	1.359	2.310	5.215	0.732	0.187	0.369
ω B97	-235.76187	1.992	2.665	5.496	-275.08203	2.000	2.678	5.515	-275.09577	1.039	2.572	5.483	1.033	0.159	0.450
ω B97X	-235.73606	1.670	2.514	5.308	-275.05318	1.676	2.445	5.350	-275.07039	1.601	2.488	5.345	1.005	0.163	0.443
BP86	-235.77918	0.633	2.013	5.036	-275.10380	0.643	2.022	4.959	-275.12301	0.759	2.061	5.089	0.034	0.431	0.299
B3P86	-235.74261	0.666	2.100	5.195	-275.06082	0.675	2.111	5.207	-275.07877	0.767	2.144	5.220	0.059	0.298	0.218
PW91	-235.66759	0.716	2.036	5.012	-274.97449	0.722	2.045	5.079	-274.99432	0.822	2.082	5.040	0.109	0.412	0.311
B3PW91	-235.71020	0.556	2.072	5.206	-275.02319	0.566	2.087	5.224	-275.04124	0.659	2.109	5.159	0.050	0.318	0.229
PBE	-235.44491	0.707	2.035	5.041	-274.71455	0.716	2.044	4.963	-274.73415	0.817	2.085	5.055	0.103	0.423	0.317
PBE0	-235.49469	0.679	2.129	5.257	-274.77241	0.687	2.137	5.272	-274.79034	0.762	2.159	5.218	0.065	0.266	0.199
PBE50	-235.55417	0.668	2.228	5.533	-274.84150	0.677	2.232	5.533	-274.85789	0.728	2.242	5.474	0.047	0.087	0.074
ω PBEh	-235.54702	0.658	2.118	5.269	-274.83346	0.667	2.126	5.285	-274.85093	0.738	2.150	5.247	0.043	0.262	0.189

^a6-311G(d) basis set.

relative number of α and β electrons. A number of parameters in B97 are fitted to thermochemical data.⁵⁸

Remarkably good performance is obtained with PBE functionals, e.g., MADs (for a large set, Fig. 7) for PBE, PBE0, PBE50, and ω PBEh are 0.21 eV, 0.13 eV, 0.09 eV,

and 0.10 eV, respectively. However, as pointed out above, using PBE50 within collinear SF-TDDFT does not improve its accuracy. We note an improved accuracy with increasing fraction of HF exchange, and that LRC (ω PBEh contains 20% short-range Hartree-Fock exchange) is superior to a sim-

TABLE IV. Total ground-state energies (hartree) and vertical excitation energies (eV) of three diradicals (unpaired electrons on opposite centers) derived by the ring opening of cyclohexane and methylcyclohexane.

	rC6r				rC6Cr ^a				rC6rC ^a				MAD		
	1A_1	3B_1	1B_1	1A_1	3A_1	1A_1	1A_1	1A_1	1A_1	3A_1	1A_1	1A_1	S-T	S-S	All
(dT) ^b	-235.00748	0.000	6.972	7.072	-274.20063	0.000	6.310	6.510	-274.20409	0.007	5.692	6.265	-	-	-
CCSD ^b	-235.00495	0.000	7.346	7.337	-274.19839	0.000	6.502	6.691	-274.20087	0.012	6.064	6.506	0.002	0.271	0.204
C-5050	-235.62918	0.000	5.177	5.181	-274.92719	-0.009	5.056	5.140	-274.93308	0.018	4.469	5.251	0.007	1.424	1.071
C-PBE50	-235.53887	0.000	5.154	5.159	-274.82503	-0.010	5.022	5.109	-274.83184	0.044	4.453	5.189	0.016	1.455	1.097
LDA	-233.56080	0.001	1.524	1.527	-272.51783	-0.002	1.459	1.566	-272.52431	0.053	1.059	1.985	0.016	4.950	3.719
BLYP	-235.64304	0.000	1.198	1.201	-274.94288	-0.008	1.144	1.227	-274.95431	0.088	0.845	1.681	0.030	5.254	3.952
B3LYP	-235.80674	0.000	2.940	2.943	-275.13370	-0.002	2.876	2.953	-275.14209	0.047	2.422	3.279	0.014	3.568	2.681
NC-5050	-235.63746	0.000	5.398	5.402	-274.93567	0.007	5.281	5.366	-274.94211	0.030	4.707	5.478	0.010	1.198	0.902
BHHLYP	-235.64453	0.000	5.308	5.312	-274.94429	0.009	5.189	5.279	-274.95096	0.036	4.628	5.396	0.013	1.285	0.968
B97	-235.71465	0.000	2.856	2.859	-275.02627	-0.012	2.774	2.856	-275.03709	0.090	2.403	3.291	0.032	3.630	2.734
ω B97	-235.74654	0.000	6.490	6.494	-275.06761	0.009	6.357	6.511	-275.07597	0.119	5.477	5.629	0.040	0.326	0.260
ω B97X	-235.73163	0.000	6.155	6.166	-275.04964	0.016	6.020	6.223	-275.06056	0.107	5.331	5.769	0.039	0.526	0.409
BP86	-235.78948	0.000	1.706	1.709	-275.11329	-0.008	1.647	1.731	-275.12190	0.051	1.255	2.097	0.017	4.779	3.591
B3P86	-235.75328	0.000	3.371	3.375	-275.07086	0.002	3.304	3.382	-275.07720	0.025	2.790	3.644	0.007	3.159	2.372
PW91	-235.67651	0.000	1.634	1.638	-274.98339	0.006	1.581	1.669	-274.99279	0.071	1.222	2.069	0.024	4.835	3.635
B3PW91	-235.72407	0.000	3.474	3.478	-275.03593	0.002	3.409	3.479	-275.04306	0.024	2.895	3.727	0.006	3.059	2.297
PBE	-235.45370	0.000	1.657	1.661	-274.72293	-0.005	1.596	1.685	-274.73223	0.067	1.232	2.078	0.022	4.818	3.622
PBE0	-235.50570	0.000	3.804	3.808	-274.78282	0.001	3.726	3.806	-274.78978	0.030	3.215	4.059	0.008	2.733	2.053
PBE50	-235.56651	0.000	5.892	5.897	-274.85275	0.000	5.751	5.845	-274.85833	0.016	5.153	5.854	0.003	0.738	0.555
ω PBEh	-235.52173	0.000	5.778	5.795	-274.84497	0.004	5.498	5.604	-274.85111	0.026	4.941	5.559	0.008	0.941	0.708

^aWe observed a large spin-contamination between the 1A_1 and 3A_1 states, in particular for the functional family B97.^b6-311G(d) basis set.

TABLE V. Total ground-state energies (hartree) and adiabatic excitation energies of TMM.

	TMM				MAD	
	3B_1	1B_1	1A_1	1A_1	S-T	All
(dT) ^a	-155.64007	0.696	0.846	3.448	-	-
CCSD ^a	-155.63248	0.788	0.918	3.761	0.092	0.159
C-5050	-155.84209	0.729	0.835	3.131	0.032	0.120
C-PBE50	-155.77283	0.739	0.846	3.142	0.043	0.116
LDA	-154.48876	0.675	0.564	1.321	0.022	0.810
BLYP	-155.87364	0.794	0.459	1.088	0.098	0.948
B3LYP	-155.96544	0.739	0.689	2.020	0.043	0.543
NC-5050	-155.85068	0.759	0.867	3.364	0.063	0.056
BHHLYP	-155.86000	0.747	0.860	3.297	0.050	0.072
B97	-155.90526	0.746	0.705	2.068	0.049	0.523
ω B97	-155.91789	0.786	0.880	3.332	0.090	0.080
ω B97X	-155.90969	0.742	0.846	3.050	0.046	0.148
BP86	-155.95492	0.727	0.576	1.490	0.031	0.753
B3P86	-155.92319	0.690	0.740	2.361	0.006	0.400
PW91	-155.88292	0.743	0.579	1.459	0.047	0.767
B3PW91	-155.90606	0.693	0.753	2.433	0.003	0.370
PBE	-155.73837	0.745	0.578	1.472	0.049	0.764
PBE0	-155.76478	0.712	0.786	2.626	0.015	0.299
PBE50	-155.79785	0.825	0.924	3.822	0.129	0.194
ω PBEh	-155.79451	0.710	0.814	2.978	0.014	0.172

^acc-pVQZ basis set.

ple hybrid (PBE0 contains 25% Hartree-Fock exchange). We also note consistently solid performance of LDA (MAD of 0.23 eV), even for relatively large systems. The distinguishing feature of PBE is that it uses exchange functional that does not include any empirical parameters and is derived to satisfy energetically significant exact relationships (the correlation in PBE is the same as in PW91). Importantly, PBE exchange restores correct linear response properties of LDA, which are compromised in PW91 exchange.⁶⁵ Since SF-TDDFT is grounded in linear response formalism, this feature is likely to be important.

Let us consider the case that was problematic for original SF-TDDFT, methylene. Figure 8 shows three adiabatic gaps computed by different methods (data from Table II). The collinear SF-TDDFT/50-50 singlet-triplet gap (green) is very poor (about -0.25 eV versus 0.42 eV). The non-collinear variant with the same functional shows little improvement (the gap becomes -0.11 eV). The best performance is observed with PBE0, PBE50, and ω PBEh; these functionals yield energy differences for all three singlet diradical states within 0.1 eV from SF-CCSD(dT).

We also note that the gaps between the singlet states, \tilde{a}^1A_1 - \tilde{b}^1B_1 (blue bars in Fig. 8) and \tilde{a}^1A_1 - \tilde{c}^1A_1 (see Table II), show much less variability and are reproduced reasonably well by all functionals. For example, the respective BLYP and PBE0 values are 0.97/1.94 eV and 0.90/2.31 eV, to be compared with 0.99/2.11 eV, SF-CCSD(dT). Thus, it appears that the SF-TDDFT errors originate in a poor description of the $M_s = 0$ component of the triplet state resulting in the energy value that is too high. This is further confirmed by energy decomposition performed in Appendix B.

The analysis of the SF-TDDFT amplitudes reveals that the character of the states is captured correctly by all methods. The spin-contamination is small for both the reference and the target states, the $M_s = 0$ component of the triplet state is a linear combination of the two open-shell configurations with almost equal weights, and the weight of the leading closed-shell configurations in the lowest singlet (1A_1) is very similar, i.e., 0.89 in SF-CCSD, 0.97 in SF/BLYP, 0.96 in SF/50-50, and 0.94 in PBE0 and LDA. Not surprisingly, the respective electron densities look very similar. Thus, we conclude that all SF-TDDFT densities are correct, and that the observed differences in performance are dominated by errors in calculating E_{ex} .

Interestingly, the open-shell singlet state, \tilde{b}^1B_1 , that has practically identical orbital character as 3B_1 does not show large errors.

Figure 9 shows BLYP transition densities for the three lowest states of methylene. Although the leading SF-TDDFT amplitudes corresponding to the configurations in Eqs. (3) and (4) are very similar (0.74/-0.68 for the singlet and 0.67/0.73 for the triplet B_1 state), the transition densities for the two states are different owing to different spin-coupling leading to different permutational symmetry of the spatial parts of the underlying wave functions. That is, the transition density for the singlet state has more nodes since the spatial part of the singlet wave function is symmetric whereas the spatial part of all triplets (whether $M_s = 1$ or $M_s = 0$) is antisymmetric. Thus, the SF transition leading to the triplet $M_s = 0$ state does not change the permutational symmetry of the spatial part of the wave function, and therefore, the transition density is more "symmetric." The transition density of the

TABLE VI. Total ground-state energies (hartree) and lowest adiabatic excitation energies (eV) in $\sigma\sigma$, $\sigma\pi$ and $\pi\pi$ diradicals.

	<i>o</i> -benzyne		<i>m</i> -benzyne		<i>p</i> -benzyne		α ,2-didehydrotoluene		α ,3-didehydrotoluene ^a		α ,4-didehydrotoluene		<i>m</i> -xylylene			MAD
	¹ A ₁	³ B ₂	¹ A ₁	³ B ₂	¹ A _g	³ B _{1u}	³ B ₂	¹ A ₁	³ B ₂	¹ A ₁	³ B ₂	¹ A ₁	³ B ₂	¹ A ₁	¹ B ₂	S-T
(dT) ^b	-230.43182	1.619	-230.41076	0.892	-230.38659	0.172	-269.44817	0.247	-269.44622	-0.066	-269.44772	0.250	-308.67947	0.454	1.116	-
CCSD ^b	-230.42486	1.578	-230.40162	0.782	-230.38010	0.147	-269.44307	0.288	-269.43960	-0.126	-269.44280	0.283	-308.67430	0.497	1.321	0.050
C-5050	-230.80751	1.883	-230.78122	0.984	-230.75495	0.164	-270.09244	0.143	-270.09338	-0.021	-270.09188	0.161	-309.43258	0.433	1.083	0.089
C-PBE50	-230.71102	1.950	-230.68780	1.141	-230.65701	0.166	-269.98518	0.246	-269.98941	0.178	-269.98453	0.263	-309.31402	0.457	1.080	0.121
LDA	-228.88022	2.058	-228.85862	1.259	-228.83071	0.454	-267.81604	0.202	-267.81605	0.019	-267.81594	0.237	-306.81368	0.295	0.622	0.199
BLYP	-230.89288	2.127	-230.87100	1.346	-230.84284	0.526	-270.18103	0.404	-270.18332	0.351	-270.17990	0.418	-309.52517	0.314	0.514	0.314
B3LYP	-230.98858	2.035	-230.96463	1.133	-230.93678	0.299	-270.30404	0.279	-270.30636	0.209	-270.30317	0.297	-309.67429	0.393	0.819	0.171
NC-5050	-230.81272	1.775	-230.78752	0.924	-230.76256	0.142	-270.10038	0.181	-270.10067	-0.042	-270.09970	0.190	-309.44023	0.446	1.132	0.054
BHLYP	-230.83701	1.807	-230.81183	0.959	-230.78606	0.147	-270.12613	0.175	-270.12678	-0.022	-270.12544	0.191	-309.46853	0.454	1.112	0.065
B97	-230.90305	1.968	-230.88183	1.216	-230.85278	0.343	-270.20576	0.374	-270.20790	0.278	-270.20416	0.392	-309.56144	0.413	0.838	0.214
ω B97	-230.91682	2.086	-230.89244	1.250	-230.85901	0.229	-270.22129	1.075	-270.22450	0.240	-270.22124	0.378	-309.58773	0.529	1.184	0.317
ω B97X	-230.90516	2.072	-230.87976	1.186	-230.84885	0.231	-270.20854	0.390	-270.21241	0.298	-270.20825	0.400	-309.57017	0.489	1.135	0.214
BP86	-230.98547	1.892	-230.96493	1.160	-230.93882	0.404	-270.29665	0.256	-270.29772	0.135	-270.29601	0.295	-309.66330	0.328	0.641	0.165
B3P86	-230.91944	1.775	-230.89689	0.990	-230.87188	0.246	-270.22538	0.219	-270.22503	0.006	-270.22488	0.244	-309.58331	0.381	0.896	0.072
PW91	-230.89359	1.930	-230.87330	1.197	-230.84624	0.417	-270.18784	0.292	-270.18941	0.190	-270.18722	0.320	-309.53641	0.327	0.626	0.194
B3PW91	-230.89738	1.745	-230.87508	0.973	-230.85034	0.231	-270.19854	0.224	-270.19796	-0.008	-270.19817	0.253	-309.55045	0.379	0.911	0.061
PBE	-230.68773	1.919	-230.66797	1.201	-230.64074	0.418	-269.94434	0.286	-269.94571	0.178	-269.94373	0.313	-309.25578	0.329	0.632	0.189
PBE0	-230.70576	1.747	-230.68390	0.985	-230.65840	0.218	-269.97201	0.230	-269.97119	-0.025	-269.97141	0.248	-309.28882	0.396	0.964	0.055
PBE50	-230.73298	1.591	-230.70857	0.776	-230.68777	0.116	-270.01152	0.299	-270.00627	-0.235	-270.01106	0.302	-309.33304	0.417	1.196	0.073
ω PBEh	-230.71788	1.889	-230.71846	0.904	-230.69334	0.177	-270.01409	0.227	-270.01289	-0.059	-270.01368	0.235	-309.33798	0.400	1.060	0.055

^aWe observed a large spin-contamination for the ³B₂ and ¹A₁ states for all functionals except C-5050, C-PBE50, and LDA.^bcc-pVTZ basis set.

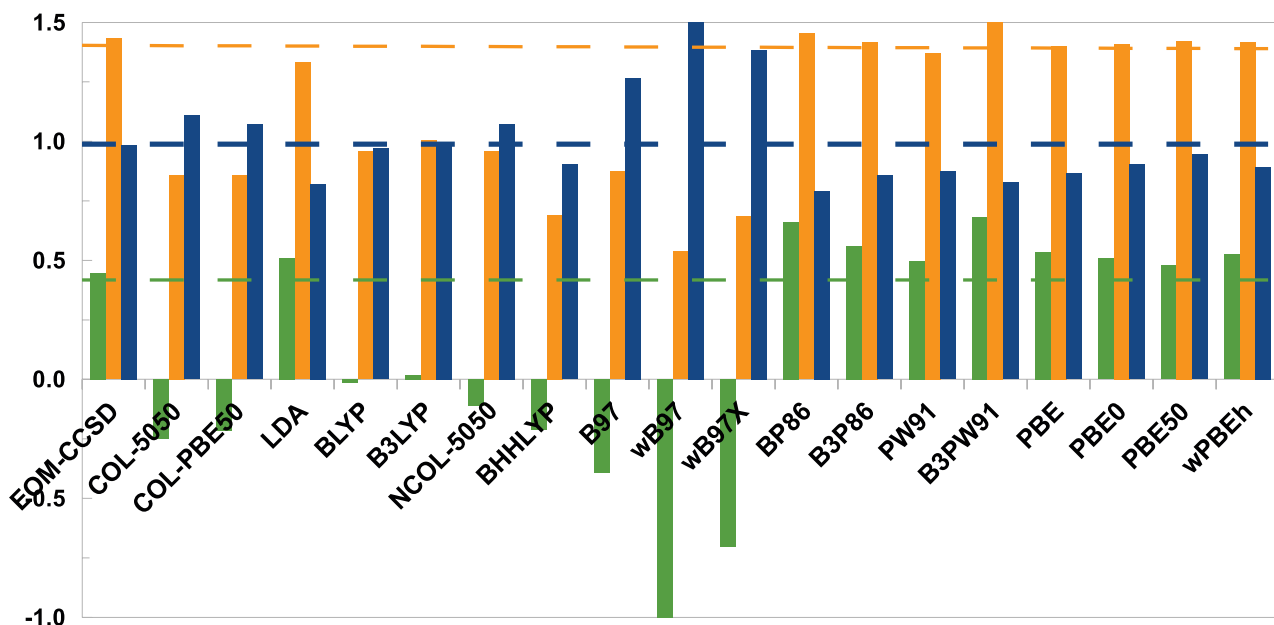


FIG. 8. Adiabatic gaps between the low-lying states of methylene (green: ${}^3B_1-{}^1A_1$, orange: ${}^3B_1-{}^1B_1$, blue: ${}^1A_1-{}^1B_1$).

closed-shell 1A_1 state has a similar nodal structure as that of 1B_1 . The amplitudes and densities for other functionals (e.g., PBE0) are very similar. Thus, the difference between different functionals is likely to be driven by the differences in the kernels along these nodes.

Other small diradicals follow a similar trend, as summarized in Fig. 10.

To further analyze the observed trends, we performed XC energy decomposition in methylene and TMM for selected functionals, as summarized in Appendix B. The results reveal that for both molecules the errors are dominated by the differences in the values of the non-collinear kernel, and that the main discrepancy is observed for the $M_s = 0$ triplet states. The BLYP values of the non-collinear contribution to total XC energy are markedly different from PBE, PW91, and PB86, which are very close to each other.

Very similar (to carbene) behavior is observed in hexane/methyl-hexane carbene-like diradicals (see Table III). We anticipate similar behavior for carbenes of variable lengths (Cnrr).

For the hexane/methylhexane diradicals in which the unpaired electrons are separated (1,6/1,7 family, see Table IV), the lowest singlet-triplet gap is reproduced relatively well by all SF methods (note that in this case, the singlet state is an open-shell like singlet). The errors for higher states are larger, which is not surprising because these higher states correspond

to charge-separated (ionic) wave functions. Thus, all DFT methods underestimate energies of these states. We observe that errors are smaller for functionals with larger fraction of HF exchange (e.g., 50-50 and BHHLYP), and for the LRC functionals. Consider, for example, the second singlet state in rC6r at 7.0 eV [SF-CCSD(dT) value]. The LDA places this state at 1.5 eV. Collinear and NC SF/50-50 energies are 5.2 and 5.4 eV. The PBE, PBE0, and ω PBEh energies are 1.7, 3.8, and 5.9 eV, respectively. The ω B97 and ω B97X values are 6.5 and 6.2 eV. Thus, states with strongly ionic character benefit from using SF with LRC functionals; however, the errors for these states are larger than for other diradicals states.

The ST gap in TMM (Table V) is accurately reproduced by all methods—the errors are well below 0.1 eV except for PBE50 (0.129 eV). However, its higher excited states are more sensitive to the functional used. The errors for higher states are smaller for functionals that use larger fractions of HF exchange, e.g., 50-50, BHHLYP, and PBE50.

For the variety of aromatic diradicals ($\sigma\sigma$, $\sigma\pi$, $\pi\pi$) from Table VI (and Fig. 11), we observe consistently good performance by all SF methods. The 50-50 and BHHLYP give MADs of 0.06 and 0.07 eV, respectively. The PBE family features the best performance. The largest errors (0.3 eV) are observed for BLYP and ω B97. The LDA MAD is 0.20 eV.

The $\sigma\pi$ diradicals present an interesting case. Because of the different nodal structure of the two frontier orbitals, the two closed-shell determinants, $(\sigma)^2$ and $(\pi)^2$, are almost uncoupled. Consequently, the two closed-shell singlet states acquire a strong zwitter-ionic character and are, therefore, high in energy. Thus, the lowest electronic states in these species are (nearly degenerate) open-shell singlet and triplet states of the $|\sigma\pi\rangle$ character. The ground state in *ortho*- and *para*-DHT is a triplet, whereas the meta isomer has a singlet ground state. We note that all SF-TDDFT methods reproduce the ST gaps in *ortho*- and *para*-DHT well. However, we observe that in the meta form a number of functionals (all

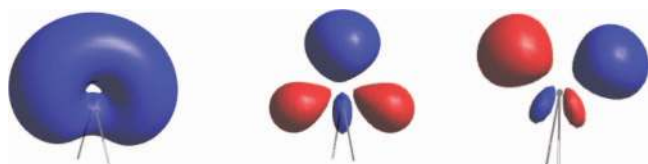
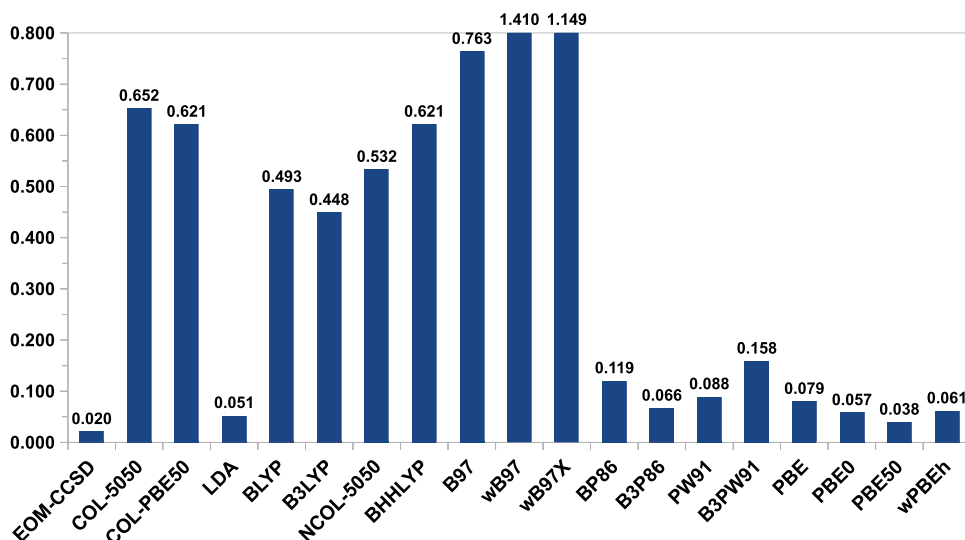


FIG. 9. Transition densities for the 3B_1 (left), 1B_1 (center), and 1A_1 (right) states of methylene.

FIG. 10. MAD (eV) of ST gaps in CH_2 , NH_2^+ , SiH_2 , and PH_2^+ .

except C-5050, C-PBE50, and NC-LDA) fail to find properly spin-coupled solutions,

$$\Psi^{t,s} \sim |\sigma\alpha\pi\beta\rangle \pm |\sigma\beta\pi\alpha\rangle, \quad (19)$$

and instead the TD-DFT equations converge to the uncoupled (and, therefore, strongly spin-contaminated) solutions, $|\sigma\alpha\pi\beta\rangle$ and $|\sigma\beta\pi\alpha\rangle$.

Finally, we would like to comment on spin-contamination in SF calculations, which needs to be monitored, and can be used as an important diagnostic. First, the $\langle S^2 \rangle$ of the high-spin reference should be checked; large spin-contamination of the reference will propagate into the response equations and spoil the description of the target states. To remedy this, ROHF references may be used. Since open-shell KS determinants are usually less spin-contaminated, the SF-TDDFT calculations seem to work fine with (slightly contaminated) unrestricted Hartree-Fock references. We would like to mention in passing that in wave function SF calculations DFT orbitals (e.g., B3LYP) can be used to mitigate spin-contamination, instead of ROHF

solutions, which are often difficult to converge. For the present benchmark set, the $\langle S^2 \rangle$ values of the reference KS determinants did not exceed 2.016, except for TMM where a slightly larger spin-contamination that increased with the amount of HF exchange was observed. The most spin-contaminated reference ($\langle S^2 \rangle = 2.075$) was observed for PBE50 (for comparison, PBE yielded 2.020).

However, even when the reference is spin-pure, the target SF states may be spin-contaminated, because the target set of the determinants is not spin-complete.^{17,18,23} This usually has little consequences for the “proper” SF states, such as diradical states discussed here (e.g., states from Fig. 3). As illustrated by the data compiled in the supplementary material,⁴⁸ the typical range of values for singlet and triplet SF-TDDFT states considered here are 0.01–0.2 and 2.01–2.2, respectively (except for *meta*-DHT discussed above). Thus, a minor spin-contamination (or, rather, spin-polarization) of the proper SF states suggests that the underlying densities are qualitatively correct and do not suffer from the unphysical extensive scrambling of different electronic states.

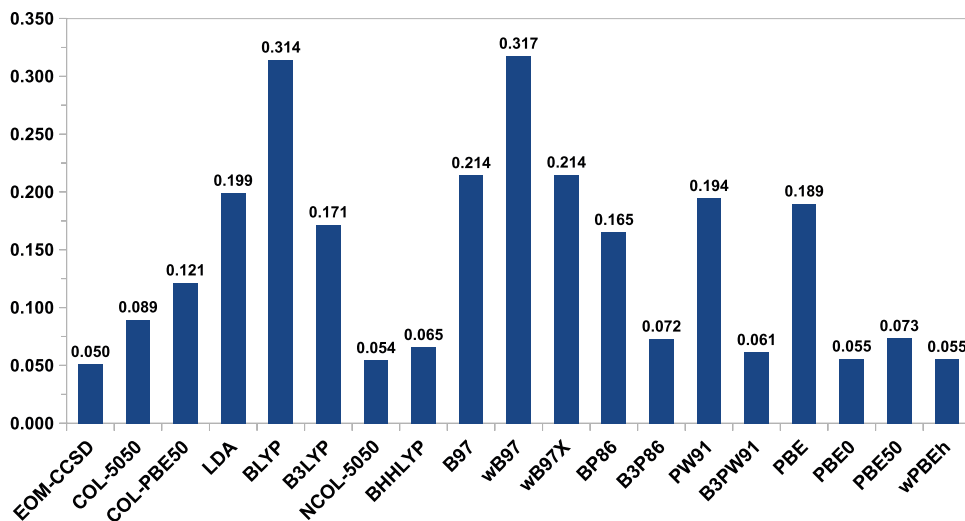


FIG. 11. MAD (eV) for ST gaps in benzynes, DHTs, and MX.

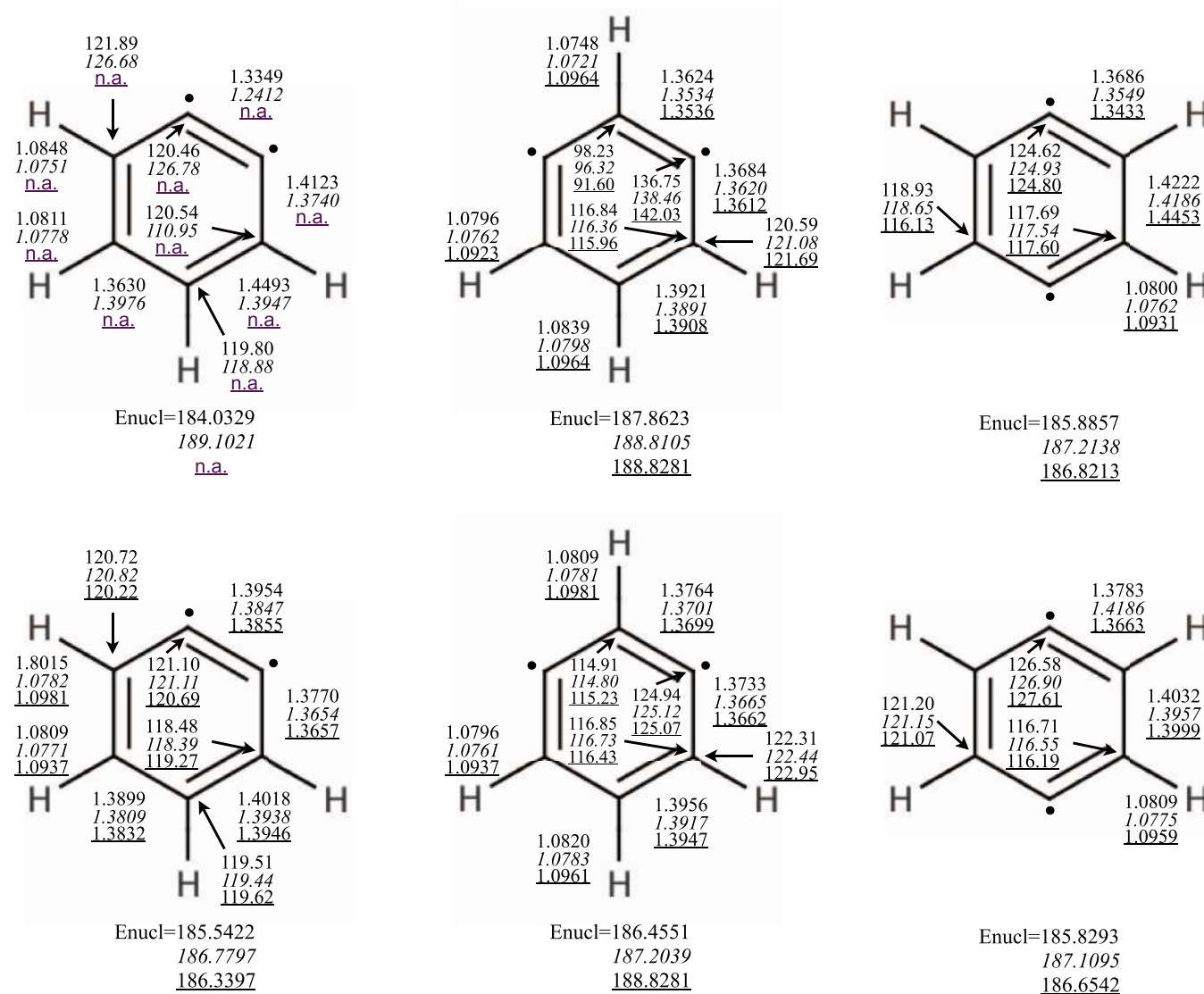


FIG. 12. Optimized geometries and nuclear repulsion energies (hartree) for the singlet and triplet states of benzyne using the SF-CCSD, COL-SF/50-50, and SF-LDA methods. Bond lengths are in angstroms, angles in degrees.

In sum, for non-carbene like diradicals, all SF-TDDFT models perform reasonably well, including collinear SF/50-50 and NC-SF/BHLYP; however, the results for the same-center diradicals show large variation. Functionals with the LYP and B97 correlation lead to much larger errors due to an overestimation of the total energy of the triplet ($M_s = 0$) state, whereas the PBE family demonstrates consistent performance for different types of diradicals. We attribute the superior performance of the PBE functionals to their accurate description of linear response of uniform electron gas⁶⁵ and the absence of empirical parameters fit to organic thermochemistry data. Excellent performance of PBE0 in TD-DFT has been noted by the original developers⁶⁶ and in a recent comprehensive benchmark study.⁶⁹

B. Structures

Collinear SF-TDDFT has been shown to yield accurate equilibrium structures of diradicals and triradicals,²⁴ which has been exploited in numerous applications^{36,38-41} including such stringent tests as modeling the photoelectron spectrum

of the *para*-benzyne anion.³⁷ The reported non-collinear SF-TDDFT/LDA structures of carbene-like diradicals (in several electronic states) were also remarkably accurate.⁴⁶ To further benchmark the performance of NC-SF-TDDFT, we optimized the structures of the singlet and triplet states of *ortho*-, *meta*- and *para*-benzyne using non-collinear SF-TDDFT/LDA and the cc-pVTZ basis. The equilibrium bond lengths and angles are presented in Fig. 12, along with the SF-CCSD/cc-pVTZ and collinear SF-TDDFT/50-50/6-311G(d) values.²⁴ All Cartesian geometries are provided in the supplementary material.⁴⁸

We observe that the performance of SF/LDA is better for relatively small systems such as carbene-like diradicals, whereas the errors for larger systems (i.e., benzyne) are larger than for original SF-TDDFT/50-50. As illustrated in Fig. 12, for these systems, collinear SF/50-50 gives better results. As suggested by the energetics (Fig. 11), non-collinear SF-TDDFT might perform better with the GGA, hybrid, and LRC functionals, especially PBE0, PBE50, and ω PBEh. Unfortunately, the analytical gradient is numerically unstable

due to the appearance of the spin-density in the denominator, which prevented us from performing geometry optimizations with non-LDA functionals. We are currently investigating different approaches for improving the numerical stability of NC-SF-TDDFT gradients.

V. CONCLUSIONS

We reported a general implementation of non-collinear SF energy and gradient for LDA, GGA, hybrid, and LRC functionals, and presented benchmark calculations of energy gaps in a variety of diradicals. The strength of SF-TDDFT is that it is a multi-state method allowing calculations of several electronic states in a single computational step. Moreover, it describes both open-shell and closed-shell singlet states on the same footing and does not rely on symmetry-broken KS solutions. It also describes systems with more extensive degeneracies such as triradicals.

The original implementation of SF employs a collinear kernel and requires large fraction of HF exchange, such as 50-50 or BHHLYP. It performs consistently well for a variety of diradicals except those in which the unpaired electrons are located on the same center (open-shell atoms, carbenes). Non-collinear SF with the 50-50 and BHHLYP functionals shows similar performance; however, the results are dramatically improved with other functionals.

The best performance for all types of diradicals is observed for the PBE family (PBE, PBE0, PBE50, and ω PBEh). The overall MADs for PBE0 and PBE50 are 0.126 and 0.090 eV, respectively.

For the same-center diradicals, LYP (BLYP, B3LYP, 50-50, and BHHLYP) and B97 (B97, ω B97, and ω B97X) functionals yield large errors (although the underlying wave functions are qualitatively correct). Interestingly, the errors originate in an overestimated energy of the $M_s = 0$ triplet state, whereas energies of other states are more accurate and consistent with other functionals. For the same-center diradicals, we observe good performance with P86 (BP86, B3P86), PW91 (PW91, B3P91), and PBE (PBE, PBE0, PBE50, and ω PBEh). With unpaired electrons on different centers, many functionals work reasonably well; PBE0 being consistently reliable. For the diradical states with large charge-separation (such as higher excited states in 1,6/1,7 diradicals derived from ring opening in cyclohexanes), the LRC functionals show noticeable improvement; however, the resulting MAD are larger than for other types of states (e.g., about 0.56 eV for ω PBEh).

We attribute the superior performance of the PBE functionals to their accurate description of linear response of uniform electron gas and the absence of empirical parameters fit to organic thermochemistry data.^{65,66}

Poor performance of B97 family suggests that different treatment of correlation between same-spin and different-spin electrons using the Stoll correction compromises the ability of these functionals to describe linear response in the spin-flipping domain.

The performance of all SF methods can be affected by spin-contamination of the reference state; however, this can be remedied by employing restricted open-shell references. None of the diradicals considered in this study showed such problems; the reference $\langle S^2 \rangle$ values did not exceed 2.1 and typical deviations from the exact $\langle S^2 \rangle$ values for the target SF states were less than 0.2 for most of the cases.

ACKNOWLEDGMENTS

This work is supported by the Department of Energy through Grant No. DE-FG02-05ER15685 (A.I.K.). Y.A.B. is supported by the postdoctoral grant from the Swiss National Science Foundation (Grant No. PBSKP2-133339). A.I.K. is a grateful recipient of the Bessel Research Award from the Humboldt Foundation supporting her sabbatical stay at the University of Heidelberg. We are grateful to Professor Mark Casida and Professor Zilvinas Rinkevicius for their help in validating our implementation. We also thank Professor Hai Wang and Enoch Dames for stimulating discussions and for drawing our attention to the ring-opening reactions in cyclohexanes and methyl-cyclohexanes. Y.S. thanks Dr. Michael Seth for helpful discussions and Professor Wenjian Liu for drawing our attention to Ref. 44.

APPENDIX A: ANALYTICAL GRADIENT FOR NON-COLLINEAR SF-TDDFT/TDA

To compute the analytic NC-SF-TDDFT energy gradient, we modified a standard TDDFT/TDA gradient procedure. One still uses the standard functional kernel in the difference density terms: $\Omega \cdot \mathbf{P}_{\omega,z}$ in Eq. (17) and $\Omega \cdot \mathbf{P}_{\omega}$ in Eqs. (19) and (24) of Ref. 47. However, the non-collinear kernel, Eq. (18), is applied in the transition density term, $\Omega \cdot \mathbf{R}_{\omega}^{\dagger}$, in Eqs. (19) and (24) of Ref. 47. Furthermore, $\mathbf{R}_{\omega}^{\dagger} \cdot \Xi \cdot \mathbf{R}_{\omega}$ in Eqs. (19) and (24) and $\mathbf{R}_{\omega}^{\dagger} \cdot \Omega^{[x]} \cdot \mathbf{R}_{\omega}$ in Eq. (21) of Ref. 47 involve functional third derivatives for the analytical gradient of standard TDDFT/TDA. With non-collinear SF-TDA, these functional third derivatives are replaced with

$$\begin{aligned} \frac{\partial^3 f_{xc}}{\partial \xi \partial \xi' \partial \xi''} \rightarrow & -\frac{1}{(\rho_{\alpha} - \rho_{\beta})^2} \left(\frac{\delta E^{xc}}{\delta \rho_{\alpha}} - \frac{\delta E^{xc}}{\delta \rho_{\beta}} \right) + \frac{1}{\rho_{\alpha} - \rho_{\beta}} \left(\frac{\delta^2 E^{xc}}{\delta \rho_{\alpha}^2} - \frac{\delta^2 E^{xc}}{\delta \rho_{\alpha} \delta \rho_{\beta}} \right) \text{ if } \xi = \xi' = \xi'' = \rho_{\alpha}, \\ & \frac{1}{(\rho_{\alpha} - \rho_{\beta})^2} \left(\frac{\delta E^{xc}}{\delta \rho_{\alpha}} - \frac{\delta E^{xc}}{\delta \rho_{\beta}} \right) + \frac{1}{\rho_{\alpha} - \rho_{\beta}} \left(\frac{\delta^2 E^{xc}}{\delta \rho_{\alpha} \delta \rho_{\beta}} - \frac{\delta^2 E^{xc}}{\delta \rho_{\beta}^2} \right) \text{ if } \xi = \xi' = \rho_{\alpha}, \quad \xi'' = \rho_{\beta}, \\ & \frac{1}{\rho_{\alpha} - \rho_{\beta}} \left(\frac{\delta^2 E^{xc}}{\delta \rho_{\alpha} \delta \xi''} - \frac{\delta^2 E^{xc}}{\delta \rho_{\beta} \delta \xi''} \right) \text{ if } \xi = \xi' = \rho_{\alpha}, \xi'' = \rho_{\alpha}^x, \rho_{\alpha}^y, \rho_{\alpha}^z, \rho_{\beta}^x, \rho_{\beta}^y, \rho_{\beta}^z \\ & 0, \text{ otherwise} \end{aligned} \quad (\text{A1})$$

within the non-collinear framework.⁴⁶

TABLE VII. Decomposition of the SF excitation energies (eV) of methylene at the 1A_1 equilibrium geometry.

	CH ₂ , 3B_1				
	BLYP	PBE	PW91	BP86	B97
H	0.66	0.06	-0.20	0.18	-0.63
J1	-0.76	-0.03	0.28	-0.17	0.80
K1	0.00	0.00	0.00	0.00	3.29
XC1	3.33	3.75	3.75	3.80	1.93
J2	0.00	0.00	0.00	0.00	0.00
K2	0.00	0.00	0.00	0.00	-3.28
XC2	-2.23	-3.23	-3.23	-3.47	-0.97
XC1+XC2	1.10	0.52	0.52	0.33	0.96
Total	1.00	0.55	0.61	0.33	1.14
	CH ₂ , 1A_1				
	BLYP	PBE	PW91	BP86	B97
H	3.96	3.17	3.32	3.70	3.75
J1	-6.25	-5.24	-5.42	-5.82	-6.08
K1	0.00	0.00	0.00	0.00	3.25
XC1	3.51	3.89	3.96	3.99	2.05
J2	0.00	0.00	0.00	0.00	0.00
K2	0.00	0.00	0.00	0.00	-2.67
XC2	-0.75	-1.22	-1.21	-1.33	-0.22
XC1 + XC2	2.76	2.67	2.75	2.66	1.83
Total	0.47	0.60	0.65	0.55	0.07
E _{ST}	-0.53	0.06	0.04	0.22	-1.07

The spin-density ($\rho_\alpha - \rho_\beta$) and, even worse, its square, appear in the denominators in the above equation, and this causes serious numerical instability in regions away from the nuclei where both α and β densities approach zero. Consequently, we could only perform non-collinear SF-TDDFT geometry optimization with LDA.

APPENDIX B: ENERGY DECOMPOSITION ANALYSIS FOR METHYLENE AND TMM

To further understand the differences between different functionals for the same-center and non-same-center diradicals, we performed energy decomposition analysis of the SF excitation energies of methylene and TMM, at their 1A_1 equilibrium geometries. The results for BLYP, PBE, PW91, BP86, and B97 (methylene only) are collected in Tables VII and VIII. The H, J1, K1, and XC1 come from $\mathbf{F} \cdot \mathbf{P}_\omega$ in Eq. (14), and correspond to the one-electron, Coulomb, Hartree-Fock exchange, and exchange-correlation components of the Fock matrix. The J2 and K2 are Coulomb and Hartree-Fock exchange parts of $\mathbf{R}_\omega^+ \cdot \mathbf{P} \cdot \mathbf{R}_\omega$. Finally, XC2 is the actual non-collinear kernel contribution, $\mathbf{R}_\omega^+ \cdot \Omega \cdot \mathbf{R}_\omega$. The total SF excitation energy (with respect to the high-spin reference) is thus the sum of all these terms. It should be noted that J2 is always zero because the Coulomb couplings between different spin-flip electronic configurations are always zero. For pure functionals, such as BLYP, PBE, PW91, and BP86 in Tables VII and VIII, the Hartree-Fock exchange contributions, K1 and K2, are vanishing too. Only for a hybrid functional B97 (which contains 19.43% Hartree-Fock exchange), the Hartree-Fock exchange terms, K1 and K2, are non-zero.

TABLE VIII. Decomposition of the SF excitation energies (eV) of TMM at the 1A_1 equilibrium geometry.

	TMM, 3B_1			
	BLYP	PBE	PW91	BP86
H	1.05	0.50	0.55	0.82
J1	-1.12	-0.49	-0.53	-0.83
K1	0.00	0.00	0.00	0.00
XC1	1.95	2.05	2.07	2.06
J2	0.00	0.00	0.00	0.00
K2	0.00	0.00	0.00	0.00
XC2	-1.17	-1.58	-1.58	-1.60
XC1 + XC2	0.78	0.47	0.49	0.46
Total	0.70	0.49	0.52	0.45
	TMM, 1A_1			
	BLYP	PBE	PW91	BP86
H	2.36	1.86	1.94	2.06
J1	-2.51	-1.85	-1.94	-2.07
K1	0.00	0.00	0.00	0.00
XC1	2.06	2.14	2.18	2.14
J2	0.00	0.00	0.00	0.00
K2	0.00	0.00	0.00	0.00
XC2	-0.72	-1.04	-1.04	-1.05
XC1 + XC2	1.34	1.10	1.14	1.09
Total	1.18	1.11	1.13	1.08
E _{ST}	0.48	0.62	0.62	0.63

As Table VII illustrates, all energy terms relatively similar for PBE, PW91, and BP86. The BLYP value of XC1 is about 0.4 eV smaller than the XC1 values of other three functionals, both in the triplet and the singlet state of methylene. However, the absolute value of XC2 for BLYP is about 1 eV smaller than for other functionals for the triplet state, whereas the difference for the singlet state is less (about 0.5 eV). Thus, the overall BLYP error in ST gap originates in the poor description of the $M_s = 0$ component of the triplet state and is driven by underestimated XC2. This is puzzling since the density and electronic character of this state seems to be described correctly, e.g., spin-contamination is low and SF-TDDFT expansion includes two leading determinants with almost equal weights, as in Eq. (3). The B97 shows large differences for both XC1 and XC2.

Although the magnitude of the error in ST gap of TMM is smaller than in methylene, energy decomposition (Table VIII) shows a similar trend: (i) the absolute values of XC1 and XC2 are smaller for BLYP; (ii) XC2 shows larger difference; (iii) the XC2 difference is larger in the triplet state.

¹T. Helgaker, P. Jørgensen, and J. Olsen, *Molecular Electronic Structure Theory* (Wiley, 2000).

²C. J. Cramer, *Essentials of Computational Chemistry: Theories and Models* (Wiley, New York, 2002).

³A. I. Krylov, *Annu. Rev. Phys. Chem.* **59**, 433 (2008).

⁴D. J. Rowe, *Rev. Mod. Phys.* **40**, 153 (1968).

⁵K. Emrich, *Nucl. Phys.* **A351**, 379 (1981).

⁶J. F. Stanton and R. J. Bartlett, *J. Chem. Phys.* **98**, 7029 (1993).

⁷H. Sekino and R. J. Bartlett, *Int. J. Quantum Chem., Symp.* **26**, 255 (1984).

⁸H. Koch, H. J. Aa. Jensen, P. Jørgensen, and T. Helgaker, *J. Chem. Phys.* **93**, 3345 (1990).

⁹M. Head-Gordon and T. J. Lee, "Single reference coupled cluster and perturbation theories of electronic excitation energies," in *Modern Ideas in Coupled Cluster Theory*, edited by R. J. Bartlett (World Scientific, Singapore, 1997).

- ¹⁰D. Maurice and M. Head-Gordon, *Int. J. Quantum Chem., Symp.* **56**, 361 (1995).
- ¹¹A. I. Krylov, *Chem. Phys. Lett.* **338**, 375 (2001).
- ¹²A. I. Krylov and C. D. Sherrill, *J. Chem. Phys.* **116**, 3194 (2002).
- ¹³A. I. Krylov, *Chem. Phys. Lett.* **350**, 522 (2001).
- ¹⁴S. V. Levchenko and A. I. Krylov, *J. Chem. Phys.* **120**, 175 (2004).
- ¹⁵A. I. Krylov, L. V. Slipchenko, and S. V. Levchenko, *Breaking the Curse of the Non-Dynamical Correlation Problem: The Spin-Flip Method*, ACS Symposium Series Vol. 958 (American Chemical Society, Washington D.C., 2007), pp. 89–102.
- ¹⁶A. I. Krylov, *Acc. Chem. Res.* **39**, 83 (2006).
- ¹⁷J. S. Sears, C. D. Sherrill, and A. I. Krylov, *J. Chem. Phys.* **118**, 9084 (2003).
- ¹⁸D. Casanova and M. Head-Gordon, *J. Chem. Phys.* **129**, 064104 (2008).
- ¹⁹L. V. Slipchenko and A. I. Krylov, *J. Chem. Phys.* **117**, 4694 (2002).
- ²⁰A. I. Krylov, *J. Phys. Chem. A* **109**, 10638 (2005).
- ²¹P. U. Manohar and A. I. Krylov, *J. Chem. Phys.* **129**, 194105 (2008).
- ²²L. V. Slipchenko and A. I. Krylov, *J. Chem. Phys.* **123**, 084107 (2005).
- ²³Z. Rinkevicius, O. Vahtras, and H. Årgen, *J. Chem. Phys.* **133**, 114104 (2010).
- ²⁴Y. Shao, M. Head-Gordon, and A. I. Krylov, *J. Chem. Phys.* **118**, 4807 (2003).
- ²⁵F. Wang and T. Ziegler, *J. Chem. Phys.* **121**, 12191 (2004).
- ²⁶F. Wang and T. Ziegler, *J. Chem. Phys.* **122**, 074109 (2005).
- ²⁷F. Wang and T. Ziegler, *Int. J. Quantum Chem.* **106**, 2545 (2006).
- ²⁸M. Huix-Rotllant, B. Natarajan, A. Ipatov, C. M. Wawire, T. Deutsch, and M. E. Casida, *Phys. Chem. Chem. Phys.* **12**, 12811 (2010).
- ²⁹Z. Rinkevicius and H. Årgen, *Chem. Phys. Lett.* **491**, 132 (2010).
- ³⁰J. A. Pople, P. M. W. Gill, and N. C. Handy, *Int. J. Quantum Chem.* **56**, 303 (1995).
- ³¹Z. D. Li and W. J. Liu, *J. Chem. Phys.* **133**, 064106 (2010).
- ³²Z. D. Li, W. J. Liu, Y. Zhang, and B. B. Suo, *J. Chem. Phys.* **134**, 134101 (2011).
- ³³Z. Li and W. Liu, *J. Chem. Phys.* **135**, 194106 (2011).
- ³⁴F. Wang and W. Liu, *J. Chin. Chem. Soc. (Taipei)* **50**, 597 (2003).
- ³⁵J. Gao, W. Liu, B. Song, and C. Liu, *J. Chem. Phys.* **121**, 6658 (2004).
- ³⁶L. V. Slipchenko and A. I. Krylov, *J. Chem. Phys.* **118**, 6874 (2003).
- ³⁷V. Vanovschi, A. I. Krylov, and P. G. Wenthold, *Theor. Chim. Acta* **120**, 45 (2008).
- ³⁸L. V. Slipchenko and A. I. Krylov, *J. Chem. Phys.* **118**, 9614 (2003).
- ³⁹L. V. Slipchenko, T. E. Munsch, P. G. Wenthold, and A. I. Krylov, *Angew. Chem., Int. Ed. Engl.* **43**, 742 (2004).
- ⁴⁰A. M. C. Cristian, Y. Shao, and A. I. Krylov, *J. Phys. Chem. A* **108**, 6581 (2004).
- ⁴¹L. Koziol, M. Winkler, K. N. Houk, S. Venkataramani, W. Sander, and A. I. Krylov, *J. Phys. Chem. A* **111**, 5071 (2007).
- ⁴²N. Minezawa and M. S. Gordon, *J. Phys. Chem. A* **113**, 12749 (2009).
- ⁴³N. Minezawa and M. S. Gordon, *J. Phys. Chem. A* **115**, 7901 (2011).
- ⁴⁴Z. Li and W. Liu, *J. Chem. Phys.* **136**, 024107 (2012).
- ⁴⁵Y. Shao, L. F. Molnar, Y. Jung, J. Kussmann, C. Ochsenfeld, S. Brown, A. T. B. Gilbert, L. V. Slipchenko, S. V. Levchenko, D. P. O'Neil, R. A. Distasio, Jr., R. C. Lochan, T. Wang, G. J. O. Beran, N. A. Besley, J. M. Herbert, C. Y. Lin, T. Van Voorhis, S. H. Chien, A. Sodt, R. P. Steele, V. A. Rassolov, P. Maslen, P. P. Korambath, R. D. Adamson, B. Austin, J. Baker, E. F. C. Bird, H. Daschel, R. J. Doerksen, A. Dreuw, B. D. Dunietz, A. D. Dutoi, T. R. Furlani, S. R. Gwaltney, A. Heyden, S. Hirata, C.-P. Hsu, G. S. Kedziora, R. Z. Khalliulin, P. Klunzinger, A. M. Lee, W. Z. Liang, I. Lotan, N. Nair, B. Peters, E. I. Proynov, P. A. Pieniazek, Y. M. Rhee, J. Ritchie, E. Rosta, C. D. Sherrill, A. C. Simmonett, J. E. Subotnik, H. L. Woodcock III, W. Zhang, A. T. Bell, A. K. Chakraborty, D. M. Chipman, F. J. Keil, A. Warshel, W. J. Herber, H. F. Schaefer III, J. Kong, A. I. Krylov, P. M. W. Gill, and M. Head-Gordon, *Phys. Chem. Chem. Phys.* **8**, 3172 (2006).
- ⁴⁶M. Seth, G. Mazue, and T. Ziegler, *Theor. Chem. Acc.* **129**, 331 (2011).
- ⁴⁷F. Liu, Z. Gan, Y. Shao, C.-P. Hsu, A. Dreuw, M. Head-Gordon, B. T. Miller, B. R. Brooks, J.-G. Yu, T. R. Furlani, and J. Kong, *Mol. Phys.* **108**, 2791 (2010).
- ⁴⁸See supplementary material at <http://dx.doi.org/10.1063/1.4714499> for the Cartesian geometries and relevant energies.
- ⁴⁹C. D. Sherrill, M. L. Leininger, T. J. Van Huis, and H. F. Schaefer III, *J. Chem. Phys.* **108**, 1040 (1998).
- ⁵⁰J. C. Stefens, Y. Yamaguchi, C. D. Sherrill, and H. F. Schaefer III, *J. Phys. Chem.* **102**, 3999 (1998).
- ⁵¹Y. Yamaguchi, T. J. Van Huis, C. D. Sherrill, and H. F. Schaefer III, *Theor. Chem. Acc.* **97**, 341 (1997).
- ⁵²T. J. Van Huis, Y. Yamaguchi, C. D. Sherrill, and H. F. Schaefer III, *J. Phys. Chem.* **101**, 6955 (1997).
- ⁵³T. Wang and A. I. Krylov, *J. Chem. Phys.* **123**, 104304 (2005).
- ⁵⁴A. D. Becke, *Phys. Rev. A* **38**, 3098 (1988).
- ⁵⁵C. Lee, W. Yang, and R. G. Parr, *Phys. Rev. B* **37**, 785 (1988).
- ⁵⁶A. D. Becke, *J. Chem. Phys.* **98**, 5648 (1993).
- ⁵⁷P. J. Stephens, F. J. Devlin, C. F. Chabalowski, and M. J. Frisch, *J. Phys. Chem.* **98**, 11623 (1994).
- ⁵⁸A. D. Becke, *J. Chem. Phys.* **107**, 8554 (1997).
- ⁵⁹J.-D. Chai and M. Head-Gordon, *J. Chem. Phys.* **128**, 084106 (2008).
- ⁶⁰J. P. Perdew, *Phys. Rev. B* **33**, 8822 (1986).
- ⁶¹J. P. Perdew, in *Electronic Structure of Solids*, edited by P. Ziesche and H. Eschrig (Akademie Verlag, Berlin, 1991).
- ⁶²J. P. Perdew and Y. Wang, *Phys. Rev. B* **45**, 13244 (1992).
- ⁶³J. P. Perdew, J. A. Chevary, S. H. Vosko, K. A. Jackson, M. R. Pederson, D. J. Singh, and C. Fiolhais, *Phys. Rev. B* **46**, 6671 (1992).
- ⁶⁴A. D. Becke, *J. Chem. Phys.* **97**, 9173 (1992).
- ⁶⁵J. P. Perdew, K. Burke, and M. Ernzerhof, *Phys. Rev. Lett.* **77**, 3865 (1996).
- ⁶⁶C. Adamo and V. Barone, *J. Chem. Phys.* **110**, 6158 (1999).
- ⁶⁷H. Stoll, C. M. E. Pavlidou, and H. Preuss, *Theor. Chim. Acta* **49**, 143 (1978).
- ⁶⁸H. Stoll, E. Golka, and H. Preuss, *Theor. Chim. Acta* **55**, 29 (1980).
- ⁶⁹S. S. Leang, F. Zahariev, and M. S. Gordon, *J. Chem. Phys.* **136**, 104101 (2012).
- ⁷⁰C. E. Moore, *Atomic Energy Levels*, National Bureau of Standards (US) Circ. No. 467 (U.S GPO, Washington, DC, 1949), Vol. 1.